Master Thesis

Temperature Simulation Model for Small Water Bodies in the Arctic Tundra, Lena River Delta (Siberia, Russia)

Karoline Wischnewski
Hermann-Elflein-Str. 34
D-14467 Potsdam

Student of Environmental Engineering at:
ETH Zurich
Rämistrasse 101
CH-8006 Zurich

Supervision:
ETH Zurich
Prof. Dr. Wolfgang Kinzelbach
Wolfgang-Pauli-Str. 15
CH-8093 Zurich

AWI Potsdam
PD Dr. Julia Boike
Telegrafenberg A43
D-14473 Potsdam

AWI Potsdam
Dr. Moritz Langer
Telegrafenberg A43
D-14473 Potsdam

AWI Alfred-Wegener-Institut für Polar- und Meeresforschung in der Helmholtz-Gemeinschaft

ETH Eidgenössische Technische Hochschule Zürich
Swiss Federal Institute of Technology Zurich

Contents

List of Figures

List of Tables

Abstract

Small and shallow water bodies are common in Arctic lowland tundra landscapes whose thermal properties differ significantly from the surrounding tundra. Water bodies recharge their heat storage during warm summer months and act as a source of heat during winter. This can lead to continuously thawed sediments below the water body (*talik*).

A dynamic one dimensional heat transport model for permafrost soils was extended to include hydrothermal processes in water. It accounts for density driven advection, wind induced mixing, absorption of light and turbulent fluxes at the water surface. Model results were validated with field data from long term measurement stations on Samoylov Island in the Lena River Delta.

Simulation results reproduced the most important features of the thermal dynamics of Arctic ponds. Shortcomings in the representation of snow cover indicated the great importance of including time varying snow thermal properties due to metamorphosis processes of snow.

Long term simulations of the thermal regime below water bodies showed that there is a threshold behaviour with respect to *talik* development. A 10-20 cm increase in water body depth evoked the sudden appearance of a *talik*. *Talik* formation was possible within the course of 2-3 consecutive years if winter conditions were comparably warm or featured a thick snow cover. The development of *talik* is triggered by the succession of these short term events rather than by long term air temperature increase.

The presented model enhances our knowledge about the susceptibility of permafrost below shallow water bodies.

1. Introduction

Climate change is one of the most important topics of today's society. Air temperature measurements over the last 50 years showed an increase of global air temperatures by 1-2°C. In Arctic regions, increase of winter temperatures was found to be even twice as much [*ACIA*, 2004]. Many changes within the arctic landscape are the results of warmer air temperatures and many of them are assumed to cause a positive feedback on global climate. Since the publication of the Arctic Climate Impact Assessment Report [*ACIA*, 2004], permanently frozen soil (permafrost) is one of the topics, which came into the focus of climate change research. The increasing air temperatures in the Arctic are associated with an increased thaw of the uppermost soil layer (active layer) during summer. As a result, formerly frozen organic matter is now available for microbial decomposition, which in turn can lead to an enhanced turnover of carbon dioxide (CO_2) and methane (CH_4) both of them highly active greenhouse gases (GHG) [*McGuire et al.*, 2009].

Peatlands and polygonal tundra are very common in arctic lowlands, feature a great number of water bodies with sizes ranging from only a few square metres up to several hectares, and store a large amount of carbon [*Boike et al.*, 2012a]. The large number of water bodies strongly influences the overall energy balance of permafrost landscapes [*Langer et al.*, 2011a]. According to the Arctic Monitoring and Assessment Programme [*AMAP*, 2011], the length of the ice cover season of lakes is reduced both by later freeze-up and earlier break-up times giving the water bodies a longer period to heat up, store energy and warm the underlying sediments. However, over 50% of the water bodies are smaller than 0.1 ha and thus are not captured by satellite images such as Landsat or MODIS [*Muster et al.*, 2012] and are therefore usually not accounted for in global climate models. Most of these ponds do not exceed a water depth of 2 m [*Wischnewski*, 2012]. These shallow ponds, as well as the underlying sediment, completely freeze during winter. If however this freeze-up cannot be accomplished during winter, related changes in ecosystem processes could be drastic. Part of the soil beneath the water body would stay unfrozen during the whole year and act as a heat source to the atmosphere during winter months [*Jeffries et al.*, 1999]. The development of thermokarst can take place during the whole year and may result in lateral growth of the water body as thaw lakes influence the permafrost not only in vertical direction [*Jorgenson et al.*, 2006; *Lin et al.*, 2010; *Plug and West*, 2009]. Methane is produced under anaerobic conditions and has a global warming potential, per mole, 3.7 times higher than that of CO_2 [*Lashof and Ahuja*, 1990]. Hence, unfrozen saturated sediment below water bodies is an environment where enhanced production would be anticipated [*Tranvik et al.*, 2009]. Current estimates of summer and fall CO_2 emissions from small ponds within the Lena River Delta were found to account for 74-81% of the net CO_2 emissions on the landscape scale [*Abnizova et al.*, 2012].

The aim of this thesis is to simulate heat transport within the water column and underlying sediments of small water bodies in the Arctic, including processes such as freeze-up, wind mixing and density driven stratification. In order to account for these processes, a one dimensional heat transfer model for soils [*Langer et al.*, 2013] is modified accordingly. With the simulations, the sensitivity of the model itself and behaviour of *talik* development is investigated.

2. Site Description

Samoylov Island (72°22'N, 126°30'E) is one of over 1500 Islands in the Lena River Delta, the largest arctic Delta which covers an area of about 29000 km^2. The delta is situated in north-eastern Siberia, Russia, at the coast of the Laptev Sea between the Taimyr Peninsula and the New Siberian Islands (Figure 2.1). Samoylov Island is located in the zone of continuous permafrost which reaches depths ranging from 500 to 600 m in the delta region [*Grigoriev*, 1960].

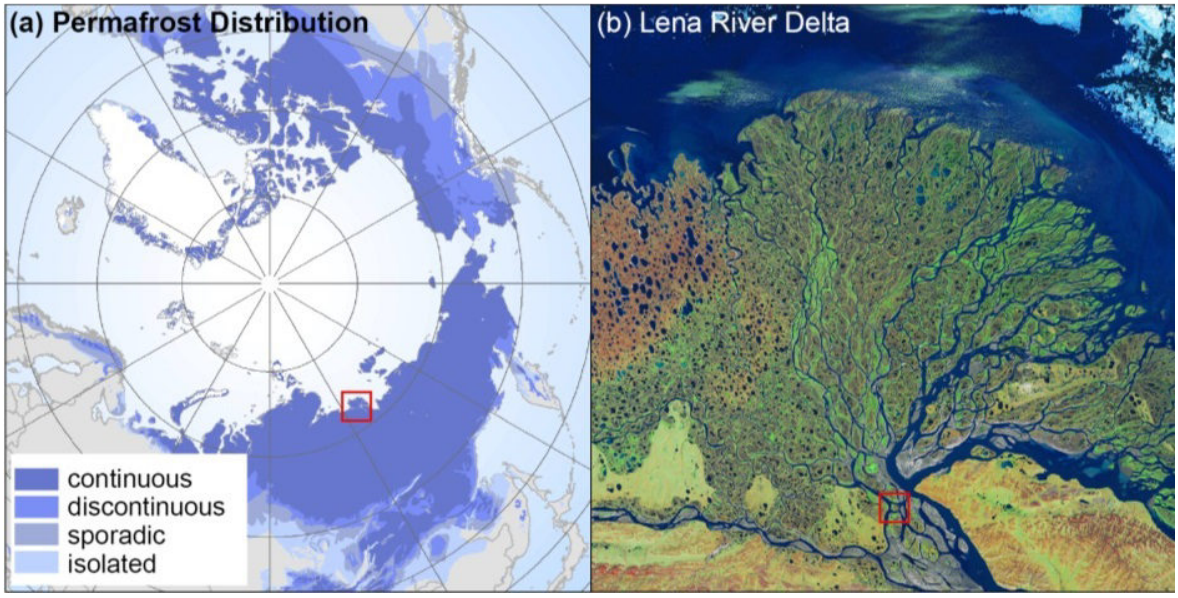

Figure 2.1 Location of study site (a) circumpolar permafrost distribution [*Brown et al.*, 1997] (b) Landsat false color image of the Lena-Delta [*NASA*, 2000]

The Lena River Delta can be divided into three terraces. The third and oldest terrace is an erosional remnant of a Late Pleistocene plain consisting of loess sediments with very high ice and organic matter content, also referred to as 'Yedoma-Ice complex'. It is the highest part of the delta and is characterised by polygonal ground and thermokarst processes. The second terrace is a complex of islands consisting of sandy sediments with low ice content and many large thermokarst lakes. It occurs in the north-western part of the delta and the largest area is represented by one island with a diameter of 110 km. The first and lowest terrace occupies most of the central and eastern part of the delta. This terrace is characterised by ice-wedge polygonal tundra, large thermokarst lakes and active flood plains. It was formed during the late Holocene [*Schwamborn et al.*, 2002]. The study area Samoylov is located on the first terrace and consists mainly of sand and peat. The dominating landform is wet polygonal tundra. During different stages of development or degradation of polygons, the centres can be low or high centred. Polygons with a high rim have a wet centre. Water levels in the centres are ranging from only a few centimetres up to 2 metres [*Wischnewski*, 2012]. The dry continental arctic climate leads to winter air temperatures as low as -50°C. The annual mean temperature measured at the meteorological station for the years 1998-2011 on Samoylov is -12.5°C and the mean annual liquid precipitation was 125 mm/y [*Boike et al.*, 2012b]. Polar night lasts from November 15 to January 28 and polar day from May 7 to August 7. The ground temperatures of permafrost at a depth of 27 m are with -8.9°C considerably colder in comparison to other arctic sites [*Boike et al.*, 2012b].

3. Background

About 24% of the northern hemisphere´s land area is underlain by permafrost [*Brown et al.*, 1997] and most of it is found in Russia and Canada. Permafrost is ground (soil or rock) with a temperature at or below 0°C for at least two consecutive years [*van Everdingen*, 1998]. The permafrost distribution is strongly influenced by the past and current climate but also depends on the glaciation history, ground characteristics, vegetation, fires, human activities and water bodies [*French*, 2007]. The uppermost layer on top of the continuously frozen sediments is called the active layer as it thaws to a specific depth during summer. In a climate as dominating on Samoylov, this layer completely freezes back during the winter months.

Figure 3.1 (a) shows a view of the Lena River Delta which is representative for the arctic polygonal tundra landscape dominating the area.

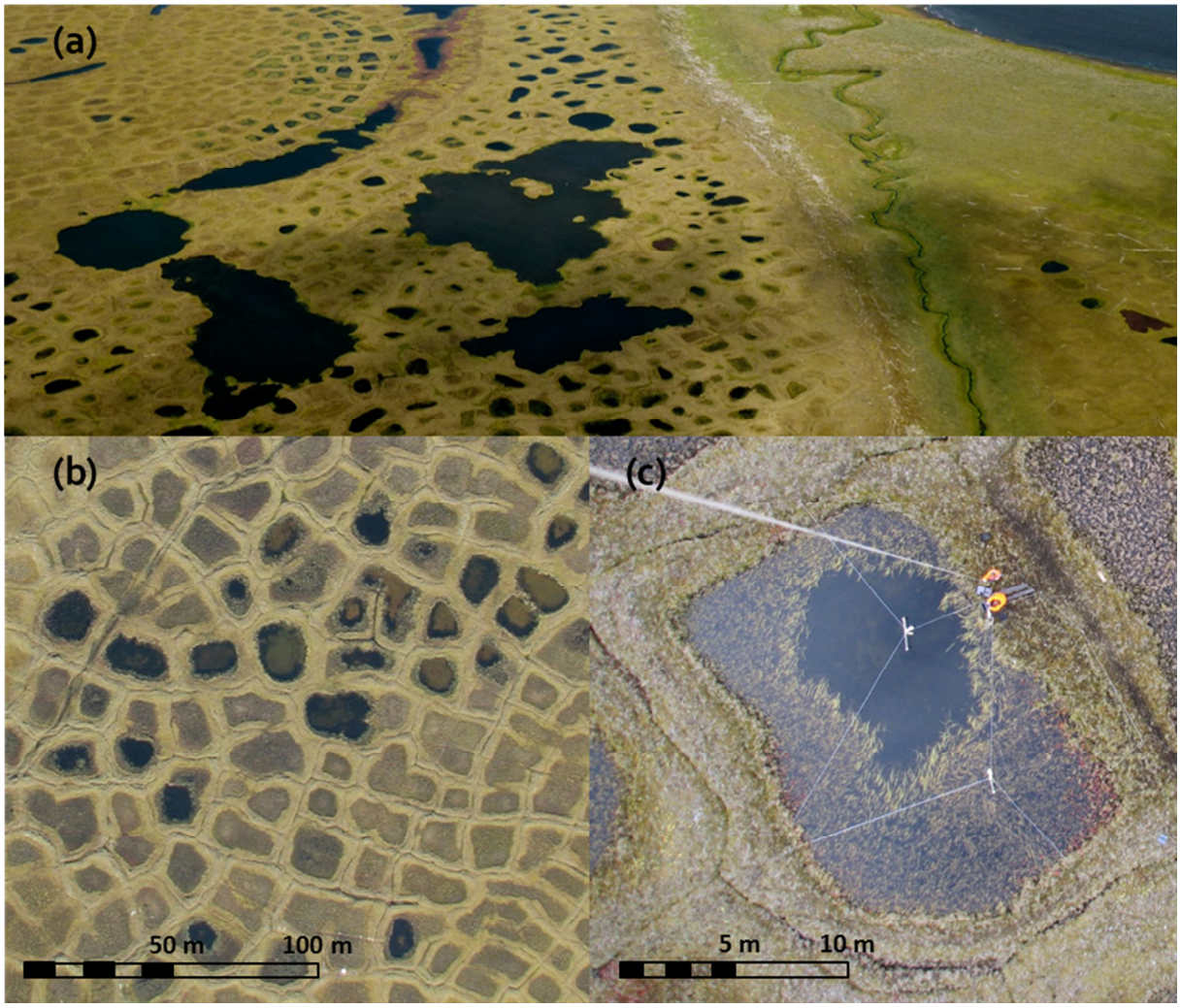

Figure 3.1 (a) Lakes, ponds an rivers in the Lena River Delta (b) open and overgrown water on Samoylov Island (c) Pond with partly overgrown water and partly open water

Peatlands, consisting of 75% wet and dry tundra and 25% water surfaces [*Muster et al.*, 2012] such as Samoylov Island, can have a protective effect on permafrost. Dry peat, which can be found on elevated rims has a low thermal conductivity and insulates underlying permafrost during the summer. Later in early winter when the peat freezes

the thermal conductivity increases significantly, hence the ground is cooled down. This seasonally varying conductivity leads to cold permafrost below peatlands [*French*, 2007]. This effect is reduced due to water bodies. The low albedo leads to a great fraction of the incoming solar radiation being absorbed within the water column. The high thermal conductivity of water in turn is conducting the heat within the water body to the underlying sediments.

Water bodies frequently occur in arctic lowland polygonal tundra. As soil is cooled down during winter months, the soil material contracts and cracks in polygonal shapes (Figure 3.1 (b) and (c)). During spring melt water is percolating into these cracks to deeper soil and refreezes where it expands and forms an ice wedge. Over many freeze and thaw cycles ice wedges grow and push up the surrounding soil [*Lachenbruch*, 1962]. The permafrost below and the intact rims above ice wedges around constrain drainage from polygon centres, transforming the tundra into a patchwork of dry rims and wet centres. Water levels in the centres range from only a few centimetres up to 1-2 metres [*Wischnewski*, 2012]. Aerial images show old polygonal structures at the bottom of larger lakes. This implies that those larger lakes might have grown from merging of smaller ponds. The small ponds can merge by a process called thermokarsting where warm water bodies melt or thaw the surrounding ice wedges or ice rich sediments respectively and can in turn connect to neighbouring polygons or grow laterally by allocation of the sediments from the sides to the bottom of the lake. Lakes evolving through this process are called thermokarst lakes [*French*, 2007].

If a water body reaches a certain depth cold winter temperatures are not low enough anymore to freeze to the bottom and water remains unfrozen throughout the year. This incomplete freeze-up affects also the underlying sediment leading to unfrozen areas throughout the year, these areas are called *talik.*

Measurements of water temperatures and meteorological parameters are simple, but become challenging in the remote and climatic extreme areas such as the high Siberian Arctic. It becomes even more challenging, when measurements of soil temperatures below water bodies are of interest. Manual installation is only possible up to a certain water level. Instrumentation of boreholes in shallow small water bodies is very invasive with a high potential for site disturbance.

In order to still be able to learn more about processes below lakes, numerical models can be a useful tool. A lot of effort has been put into modelling heat transport for lakes in temperate zones [*Cathcart and Wheaton*, 1987; *Mironov*, 2008; *Riley and Stefan*, 1988]. Ice cover in those models is often, if at all, represented in a very crude manner and complex freeze and thaw processes of the underlying sediment are not an issue for non-permafrost lakes and therefore not at all accounted for in those models. In an environment, where freeze and thaw is occurring during the greater part of spring to autumn this process cannot be neglected. Timing of ice break- and freeze-up is a crucial factor for heat storage in *taliks* below lakes as the warm period is very short and wrong timing can result in great errors for the overall energy balance.

3.1. Thermal Dynamics of Small Water Bodies

In advance to this thesis a study of the thermal dynamics of arctic ponds and lakes was carried out and presented in the framework of a project thesis [*Wischnewski*, 2012] and in [*Boike et al.*, 2012b]. The results of this study are presented shortly in order to give a notion of important features of water bodies in the arctic.

Water bodies on Samoylov were separated according to their surface area and their water depth into 4 classes (Table 3.1).

Table 3.1 Nomenclature for water bodies

Area	Depth	Description
<0.1 ha	<1 m	shallow pond
<0.1 ha	>1 m	deep pond
0.1 ha-10 ha	<3 m	shallow lake
0.1 ha-10 ha	>3 m	deep lake

A survey of 103 ponds on Samoylov Island showed that water depth ranged between a few centimetres up to 1.3 m. Only three lakes were studied with depths from 3.4 - 6.1 m. Ice cover build up started in end-September for all water bodies. The ponds took about 3-4 months to freeze to the bottom and lakes developed a maximum ice-thickness of ~2 m hence, lakes did not freeze completely. Start of ice melt at the shorelines of lakes was seen from temperature increase at sensors in lower water layers in the centre of the lake, before the sensor at the surface in the centre of the lake reached temperatures above 0°C. It took about 2 months to melt the ice completely. The time for melting ice cover of ponds was considerably shorter with only 1 month. In the end of May temperatures increased nearly isothermal up to 0°C, were refrozen for a short period and after that entered simultaneously the zero curtain. The zero curtain is a timespan during which temperatures stay at or fluctuate around zero due to phase change from the frozen to the liquid state. At the end of May water surface temperatures climbed above 0°C and bottom temperatures followed just 2-3 days later.

One feature which was observed in ponds as well as in lakes was an increase of bottom temperatures as soon as ice cover was built up at the surface. At that point the water column was observed to be isothermal at nearly 0°C. Afterwards temperatures started to increase again. This increase of temperatures was observed to be strongest at the bottom of the pond and suggested that this increase was resulting from heat input from underlying warmer sediments.

4. Heat Transport Model

4.1. Model Formulation

The model used in this work is based on a 1D heat transport model for soil [*Langer et al.*, 2013]. The soil was described by vertically stacked cells with varying compositions of sand, mineral and organic material. The remaining pore volume was saturated with water. The model solves the one-dimensional heat transfer equation [*Sophocleous*, 1979]

$$C_{app}\frac{\partial T}{\partial t} - \frac{\partial}{\partial z}\left(k_h \frac{\partial T}{\partial z}\right) = 0\,, \tag{1}$$

where T is the water temperature as a function of depth z and time t, k_h is the thermal conductivity. C_{app} is the apparent heat capacity, a term combining the heat capacity C_h and the energy turnover related to phase change [*Yershov and Williams*, 1998] calculated as

$$C_{app} = C_h + \rho_w L_v \frac{\partial \Theta_w}{\partial T}\,, \tag{2}$$

Θ_w is the liquid water content of the soil, which changes with the temperature T, L_v the latent heat of fusion and ρ_w is the density of water.
Calculations for the heat capacity and thermal conductivity are following an approach from [Campbell et al., 1994; De Vries, 1966]. The calculated thermal conductivity following other approaches [*Endrizzi et al.*, 2011; *Johansen*, 1975] has been compared by [*Fröb*, 2011] and the results showed the best fit of calculating the thermal conductivity of soils on Samoylov following the approach from de Vries. Equations read as follows

$$C_h = \sum_j \Theta_j\, C_j\,, \tag{3}$$

$$k_h = \frac{\sum_j \Theta_j\, f_j k_j}{\sum_j \Theta_j\, f_j}\,, \tag{4}$$

with the indices j for *water*, *ice*, *mineral* and *organics*, Θ the volumetric fraction of the material and C the specific heat capacity. Thermal conductivity calculations also take into account the parameter f, which merges shape factors for soil particles and threshold values for soil water circulation.
The freeze curve calculation for liquid water content of soil was done by using the following empirical equation

$$\Theta_w(T) = \begin{cases} \Theta_{w(\min)} & for\ T < 0 \\ \Theta_{w(\max)} + \frac{\Theta_{w(\max)} - \Theta_{w(\min)}}{1 - AT + BT^2} & for\ T \geq 0 \end{cases}, \tag{5}$$

$\Theta_{w(min)}$ and $\Theta_{w(max)}$ are minimum and maximum liquid water content of the soil. The empirical parameters a and b are site specific and can be found via fitting measured data of the site to the second order polynomial shown above [*Langer et al.*, 2011a].

The heat transfer Equation (1) is discretised for numerical solutions following a central difference scheme. This results in a set of ordinary differential equations, each one describing the energy change in a corresponding cell of the model. Cells are fine gridded

at the surface (2 cm steps) and grow coarser below 2 m. The model is implemented in Matlab® and uses an internal function to solve the system of ordinary differential equations (ode15s) which works on a flexible time integration. This was changed in the adapted version to a fixed time step of 10 seconds.

4.2. Model Modifications

Water body

The first step for changing the soil model to a lake model was to include cells consisting purely of water overlying the soil cells. The existing model was interpolating soil compositions for given horizons. A cell consisting of water was then created by setting fractions for mineral and organic soil to zero. As described above, the liquid water content is following a specific freeze characteristic which in turn affects the thermal conductivity. Thermal conductivity of water on the other hand can be approximated by two values, one for the frozen and one for the unfrozen state. This change in thermal conductivity for water was for numerical reasons described by a simple *arctan*-function. Figure 4.1 shows the conductivities as used in the temperature simulation model.

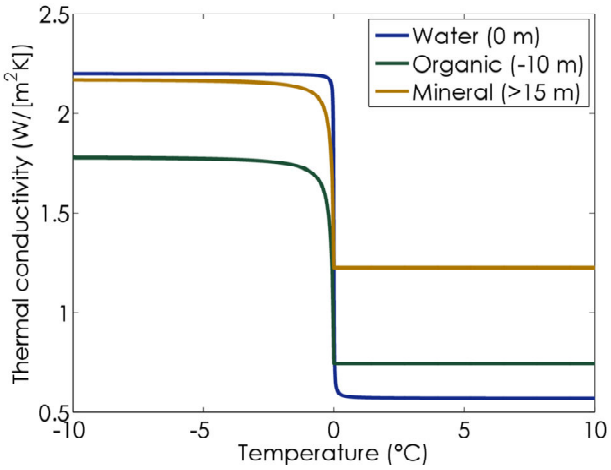

Figure 4.1 Thermal conductivity in dependence of temperature for pure water (blue), organic sediments (green) and mineral soil (ochre)

Values for thermal conductivity and heat capacity were calculated for every cell for the temperature range from -10 to 10 °C and were saved to be accessible as look up tables during calculations. So far, only conductive transport was represented in the model. Advective heat transfer which plays a key role for the heat transfers in liquid water was parameterised as follows:

Density driven advection

Water has its highest density at *3.98 °C* which can induce density driven advection. For deeper lakes this can lead to thermal stratification if wind induced mixing is not affecting deeper layers of the lake. Floating ice during the winter months is also a result of density difference, as ice is much lighter than liquid water. Density of water was calculated with the polynomial function [*Kell*, 1975]

$$\rho_w(T) = \frac{a_0+a_1T+a_2T^2+a_3T^3+a_4T^4+a_5T^5}{1+bT}, \quad (6)$$

for T greater than zero degrees Celsius with the coefficients a_0, a_1, a_2, a_3, a_4, a_5 and b (see annex A.1). The density for water below 0°C was assumed to be constant at $916.7\ kg\ m^{-3}$. The density was calculated each time step for every water cell. In the model, the cells were then sorted according to their density. Due to the lower density of ice the cells with temperatures below 0°C float above the remaining liquid cells. This opposes field observations of shallow ponds which froze to the bottom during winter. During spring melt the ice does not ascent to the top because it is frozen to the ground. Instead the water pools on top. This process was implemented as follows: if the cells directly above and below the water soil interface were frozen during spring melt all frozen cells were excluded and only overlying liquid water cells were sorted.

Wind induced mixing

Wind induced mixing of the water bodies was also included and made use of an integral energy approach introduced by [*Ford and Stefan*, 1980]. This approach uses turbulent kinetic energy (*TKE*) supplied by wind to work against the gravity force of a mixed layer. Turbulent kinetic energy is calculated as

$$TKE = \rho_w u^* A_s \Delta t, \tag{7}$$

where ρ_w is the density of the mixed layer, A_s the surface area of the modelled lake and Δt the time step. u^* is the shear velocity of the water due to wind (see annex A.2). In order to decide whether a certain layer is entrained or not, the *TKE* had to be larger than the work required to lift the mass of this layer to the gravitational centre of the mixed layer:

$$W_L = V_m \Delta\rho g (z_{mix} - z_g), \tag{8}$$

with V_m the volume of the mixed layer, $\Delta\rho$ the density difference of the layer of question and the mixed layer, z_g centre of gravity of the mixed layer, z_{mix} depth of the mixed layer and g the acceleration of gravity. As long as *TKE* was larger than W_L the thermal conductivity of the entrained cell was enhanced by

$$k_h = k_w + K_z C_w, \tag{9}$$

with k_w the thermal conductivity of water, C_W the heat capacity of water and K_z the hypolimnetic eddy diffusivity [*Hondzo and Stefan*, 1993]

$$K_z = \omega (N^2)^{-0.43}, \tag{10}$$

With ω a scaling factor related to the general level of turbulence ($6.9*10^{-6}$) and N^2 the Brunt-Vaisala frequency which determines the stability of the water column and is given by

$$N^2 = -\frac{g}{\rho}\frac{d\rho_w}{dz}. \tag{11}$$

If *TKE* was not large enough to lift one cell *TKE* was dissipated as internal energy to the appropriate cell.

Wind induced mixing only occurs when the lake is not covered by ice. The lake was considered ice free when the uppermost water cell exceeded a temperature of 0.5°C.

Snow Cover insulation

The seasonal snow cover is an important component in the soil atmosphere system and was also included in the soil model. However, since snow changes its thickness during the course of a year and the model does not work on a flexible spatial grid a fixed grid with changing properties was "stacked" on top of the water cells. Those additional cells are referred to as "air cells" but do not calculate air temperatures, but were forced to take on the measured air temperature.

The model expects a known snow depth for the whole simulation period as an input parameter (see chapter 4.4) which was then translated to a number of air cells being transformed to snow cells. Snow cells could only be formed, if the condition of a frozen water surface was fulfilled. Thermal properties were then assigned to the newly formed snow cells and were taken to be constant until the cell was removed. Thermal conductivity was taken as 0.2 W m^{-2} K^{-1} and the heat capacity was calculated after [*Goodrich*, 1982] with a constant snow density ρ_s of 250 kg m^{-3} [*Riche and Schneebeli*, 2013] as follows

$$C_s = 2.09 * 10^3 \rho_s \,, \tag{12}$$

The changes of snow properties due to metamorphosis processes were neglected.

Energy Balance

The surface energy balance was calculated for every time step and acts as a source/sink term for the uppermost cell in the model which can either be a water, ice or snow cell. The energy balance consists of radiative, turbulent and ground heat fluxes. The energy balance equation reads as follows

$$Q_{net} - Q_H - Q_E - Q_G = 0 \,, \tag{13}$$

with net radiation Q_{net}, ground heat flux Q_G, latent heat flux Q_E and sensible heat flux Q_H. The net radiation is calculated as

$$Q_{net} = (1 - \alpha) Q_{SW\downarrow} + \varepsilon Q_{LW\downarrow} - \varepsilon \sigma T_{surf}^4 \,, \tag{14}$$

with α the surface reflectivity (albedo), $Q_{SW\downarrow}$ the incoming short wave radiation and $Q_{SW\downarrow}$ the incoming long wave radiation. ε is the surface emissivity (depending on surface material), σ the Stefan-Boltzmann constant and T_{surf} the surface temperature which was taken from the previous time step during calculations. The sensible heat flux follows can be obtained by e.g. [*Van Bavel and Hillel*, 1976]

$$Q_H = -C_a \frac{1}{r_a} \left(T_m - T_{surf} \right) \,, \tag{15}$$

where C_a specific heat capacity of air, T_m temperature at measuring height, T_{surf} temperature at the water surface and the aerodynamic resistance r_a

$$r_a = \frac{\left[\ln\left(\frac{z_m}{z_0}\right)\right]^2}{\kappa^2 u_{zm}}, \tag{16}$$

with u_{zm} wind speed at measuring height, κ the von Kármán constant (0.4) and z_o=10^{-4} m the roughness length for a calm water surface [*Garratt*, 1994]. Equation (16) is only valid for neutral atmospheric conditions. It has been shown that these conditions are usually fulfilled during summer months on Samoylov Island [*Langer et al.*, 2011b]. The latent heat flux Q_E can be obtained from [*Garratt*, 1994]

$$Q_E = \frac{-\rho_{air} L_v}{r_a}\left(q(z_m) - q\left(z_{surf}\right)\right), \tag{17}$$

with ρ_{air} the temperature- and humidity dependent density of air (see annex A.4), L_v the latent heat of vaporization. $q(z)$ is the specific humidity at measuring height z_m and at the water surface z_{surf} and was obtained as follows

$$q\left(z_{surf}\right) = 0.622 \cdot \frac{p_d}{p}, \tag{18}$$

$$q(z_m) = 0.622 \cdot \frac{p_d}{p} \cdot RH, \tag{19}$$

p_d is the partial pressure (see annex A.4), p is the atmospheric pressure and *RH* the relative humidity at measuring height.

Resulting from equation (13) the ground heat flux Q_G was then calculated as the residual of the net radiation and turbulent heat fluxes and acts as an energy source (or sink) to the upper most cell of the model (either snow, water or ice).

Solar Radiation

In an environment of polar night and day the influence of incoming solar radiation is very important. When shortwave radiation meets the surface part of it is reflected. This surface reflectance (albedo) strongly depends on the surface material. Surface absorption is also depending on the surface material (see annex A.1) and takes place within the first centimetres below the surface. This results in the two following equations for net shortwave radiation within the two uppermost cells [*Riley and Stefan*, 1987]

$$Q_{SWnet(z(1))} = (1-\alpha)(1-\beta)Q_{SW\downarrow}\, e^{-kz} + \beta Q_{SW\downarrow}, \tag{20}$$

$$Q_{SWnet(z(2))} = (1-\alpha)(1-\beta)Q_{SW\downarrow}\, e^{-kz} \tag{21}$$

with α the surface reflectance, β the surface absorption both depending on surface material (cp. annex A.1) and $Q_{SW\downarrow}$ the incoming shortwave radiation. Below the surface, net solar radiation with depth follows Beer´s law for attenuation of light

$$Q_{SWnet(z(i))} = Q_{SWnet(z(i-1))} e^{-kz}, \tag{22}$$

with k the extinction coefficient of the penetrated material (annex A.1).

4.3. Boundary & Initial Conditions

After all modifications the heat flux equation reads as

$$\left(C_h + \rho_w L_v \frac{\partial \Theta_w}{\partial T}\right)\frac{\partial T}{\partial t} = \frac{\partial}{\partial z}\left((k_h + K_z C_w)\frac{\partial T}{\partial z}\right) + \frac{\partial \Phi}{\partial z}, \quad (23)$$

Compared to the previous soil version, the effective thermal conductivity was increased by the effect of eddy conductivity $K_z C_w$ (set to zero in soil cells) and the energy source Φ resulting from the short wave radiation penetrating into water layers. The model is simulating temperatures on a vertical column from 1.2 m to -500 m. Altogether 180 grid cells were being modelled with a spacing of 0.02 m between 1.2 m and -2 m and increasing cell size to a maximum of 20 m at the bottom of the column. In the case of deeper water bodies the fine gridded cells of 0.02 m thickness were adjusted accordingly. The upper 1.2 m is occupied by 'air cells' followed by a varying number of water cells depending on modelled water depth. The remaining cells are soil cells with varying soil composition (Table A.2 in annex A.2). At the bottom cell the model was forced with a geothermal ground heat flux as the lower boundary. This flux was set to $53e^{-3}$ W m^{-2} [*Langer et al.*, 2013]. At the surface the model was forced with the measured air temperature, the calculated ground heat flux and the absorbed fraction of Q_{SW} (equations (13) & (20)).

Table 4.1 Initial conditions

Depth (m below WS)	0	0.7	0.9	1.1	1.2	20	500
Temperature (°C)	4.4	4.7	4.7	1.9	0	-10	0

Initial conditions for model set up were interpolated from values given in Table 4.1, where temperatures of the depths 0-1.1 m are measurements from the water profile at the pond site 'M003' (cp. Figure 4.2) at the actual start date of the set up period. The active layer depth at 1.2 m is taken from field measurements in July 2012. Permafrost is considered to end at 500 m depth.

4.4. Forcing Data

Long term observational data

As mentioned before all forcing data (except snow depth) for the model was taken from long term observation sites on Samoylov Island. The Alfred Wegener Helmholtz Centre for Polar and Marine Research has instrumented several stations on the island starting in 1998 (see Table 4.2 [*Boike et al.*, 2012b]).

Table 4.2 Overwiev of available data

	Height	Sensor	Time span
Temperature	2m	Campbell HMP45c	1998-2012
Humidity	2m	Campbell HMP45c	1998-2012
Wind speed	3m	RM Young 05305	1998-2012
4 component radiation	2m	Hukseflux NR01	2010-2012
Surface Temperature	0.3m	Campbell IRTS-P	2006-2012
Snow Depth	0.8m	Campbell SR50A	1998-2012
Automatic Camera	3m	Campbell CC640	2006-2012
Water Temperatures Lakes	Profile	HOBO U22-001	2009-2012
Water Temperatures Ponds	Profile	HOBO U22-001	2010-2012
Water Temperatures Pond	Profile	PT100	2006-2012

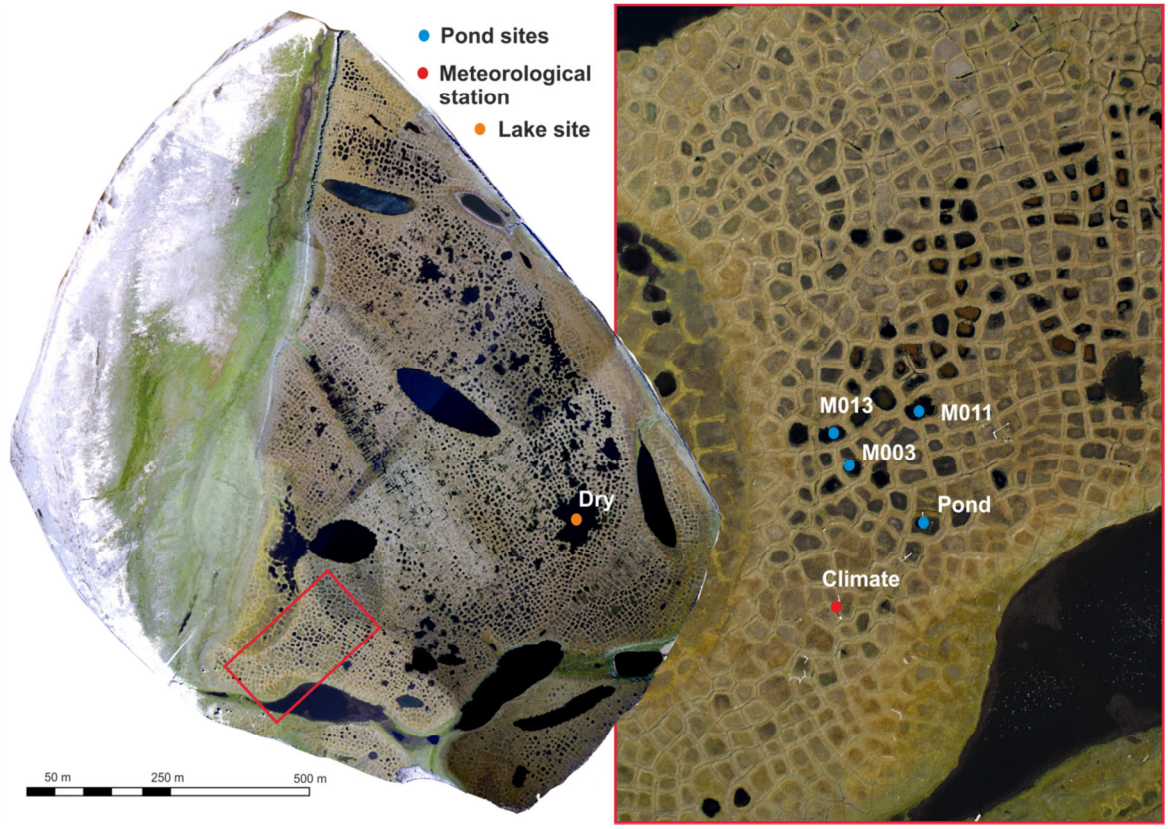

Figure 4.2 Observation sites on Samoylov Island

The quality of the data is very good although some outliers and gaps during the period 1998-2010 did appear. Those gaps were filled with ERA-Interim reanalysis data [*Mooney et al.*, 2011; *Screen and Simmonds*, 2011]. For humidity no reanalysis product was available. A simple autoregressive method was applied synthesizing data from the monthly average plus a random variable times the standard deviation of the data. The resulting time series are shown in the annex A.5. The snow depth for the years 1998 to 2010 was calculated with a constant density of 250 kg m^{-3} and snow water equivalents taken from the GlobSnow product which had data available since 1979 and gave daily values with a spatial resolution of 25 km [*Luojus et al.*, 2010; *Takala et al.*, 2011]. GlobSnow is a product based on measurements from two space-borne passive microwave sensors (SMMR and SSM/I) and combines these time series with field data from stations on the ground [*Pulliainen*, 2006]. It has been shown by [*Langer et al.*, 2013], that accuracy of GlobSnow SWE data is adequate for tundra lowland landscapes. For the period 2010-2012 snow depth from the observation site was used. For calibration and validation purpose temperature profiles of a number of ponds and lakes (see Figure 4.2, Table 4.3) are used from the years 2010 to 2012.

Table 4.3 Overview of depth and area of instrumented water bodies

Description	Depth	Area
Lake 'Dry'	3.4 m	23066 m^2
Pond 'M003'	0.81 m	164 m^2
Pond 'M011'	1.21 m	248 m^2
Pond 'M013'	1.27 m	175 m^2
'Pond'	0.86 m	178 m^2

Surface temperature measurements from an infrared surface temperature sensor and pictures from an automatic camera (1 shot per day at noon) were used for feasibility check of model input.

Model Set Up, Long Term Simulations & Validation

Emphasis was placed on the thermal dynamics of shallow ponds and therefore model design and set up was done for a shallow pond with a depth of 81 cm. Simulation results were compared with measurements originating from the pond site 'M003' (cp. Figure 4.2, depth: 0.81 m) for the years 2010 to 2012.

In order to test for sensitivity of snow cover additional runs with simplified conditions were conducted. The upper boundary consisting of air temperature and the surface energy balance was replaced by measured water surface temperatures. In this case, there was no need to include snow cover but density driven stratification, wind induced mixing and absorption of incoming short wave radiation in deeper water layers was considered.

The next step was to conduct long term simulations which were done with input data from the years 1998 to 2010. A depth range from 0.4 to 2 m (10 cm steps) was chosen since the critical depth for *talik* development was expected within that range. An additional run for the depth 3.4m was carried out to test the model's applicability for deeper lakes. This validation was done by comparison of model output with the measured temperature profile of the lake site 'Dry'.

With resulting water temperature profiles after long term simulations the new initial conditions were set for the validation period from 2010 to 2012.For that period the simulation results were compared to measured temperature profiles of the water bodies pond 'M011' & 'M013' with depth 1.21 m and 1.27 m respectively.

To test for susceptibility of the thermal regime below the water bodies, a future scenario for 20 years was conducted with a gradual temperature increase of 0.1°C per year for water bodies with depths 1.41 m, 1.51 m and 1.61 m. Air temperatures for this scenario were synthesised from a random pick of previous annual cycles to which the temperature increase was added. Snow cover, wind speed and other input variables were also randomly put together from previous years but without modification.

The model performance was evaluated using the coefficient of determination R^2

$$R^2 = 1 - \frac{\sum_i (Y_i - \hat{Y}_i)^2}{\sum_i \left(Y_i - \overline{Y}_i\right)^2}, \tag{24}$$

with Y_i the measured value, $\hat{Y}_i$ the modelled value and $\overline{Y}_i$ the mean of the measured values.

5. Results

5.1. Simulation Results for Ponds

Pond 'M003' – Setup of Model

Results for the water temperature simulation with the surface energy balance and measured air temperatures as the upper boundary condition in daily resolution for a pond with a water depth of 0.81 m are shown together with measured water temperatures of pond 'M003' in Figure 5.1.

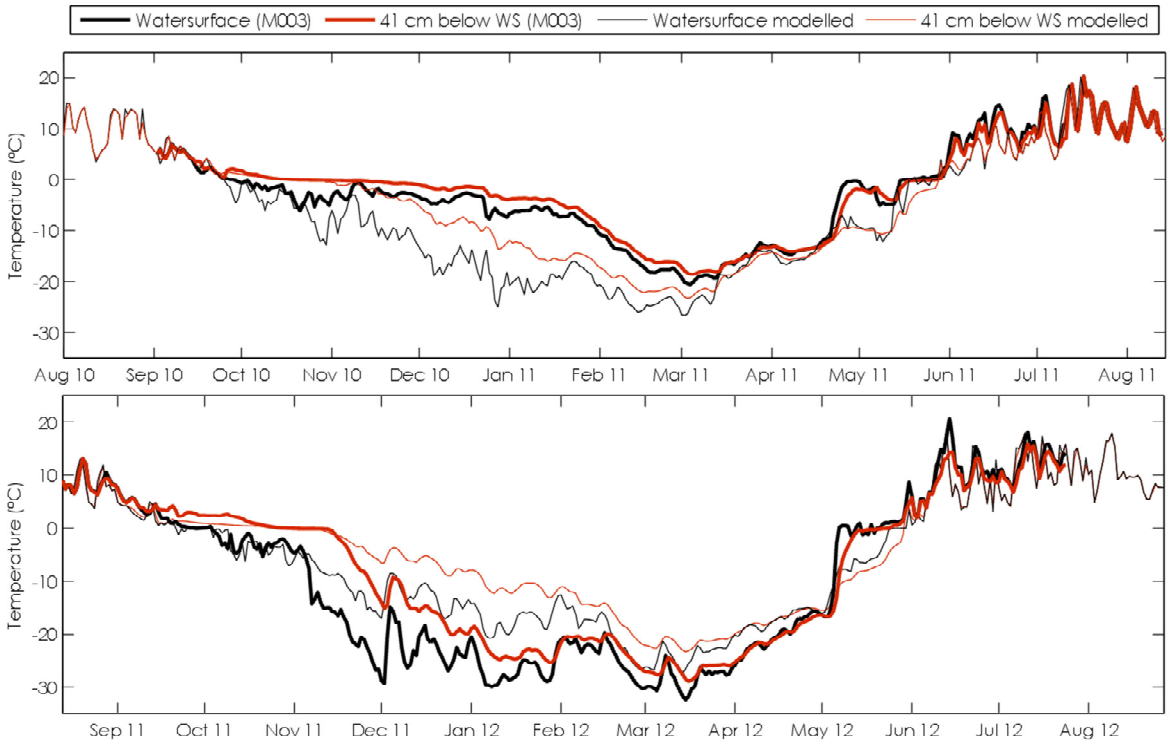

Figure 5.1 Comparison of modelled (thin) and measured (thick;M003) temperatures at the water surface (black) and 41 cm below the water surface (red) for a pond with a depth of 81 cm, 2010-2011 (upper figure) and 2011-2012 (lower figure).; upper Boundary: Air Temperature & Energy Balance

An overall R^2 of 0.3755 between modelled and measured water temperatures was achieved. Temperatures from March until end of September were simulated in an acceptable manner but generally slightly underestimate measured temperatures for both years. Modelled temperatures in the year 2010/11 from October to February deviated up to 20 degrees and during May temperatures for both years deviated 5-10 degrees from observed data. Although the results of the simulations show a zero curtain during freeze-up, the length of this period was different for both years. The gradients on decreasing temperatures during November are either too steep or too shallow for the two years respectiveley. From October to end of December in 2010 modelled temperatures dropped from zero to below -20 °C whereas only a small decrease of temperature was observed in the measured data. Responses to air temperatures appeared to be much more dampened than the modelled reaction. Modelled and measured values aligned again in early February for both years. Whereas winter temperatures for the first year were underestimated, the simulated temperatures in the

second year were warmer than observed temperatures. In May, during ice break-up the modelled temperature curves did not rise as quickly as the measured curves. Temperature rise in 2012 started at 4th of May with a steep gradient but when measurements kept on rising simulated temperature rise ceased midway and stayed at around -7°C until 27th of May. Then, they increased again and met the measured temperatures, which were just around zero degrees for this period. A similar development was observed in the previous year.

Pond 'M013' & 'M011' – Validation

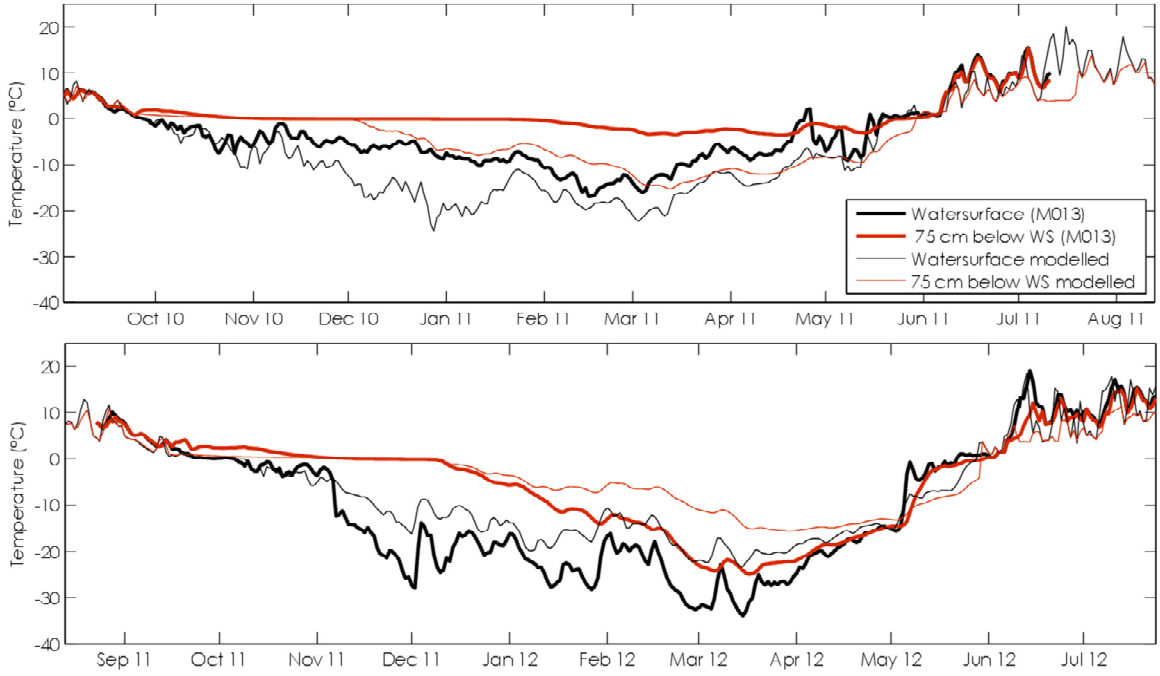

Figure 5.2 Comparison of simulated (thin) and measured (thick) temperatures of a pond 'M013' with depth 1.28 m, at the surface (black) and at 76 cm below water surface (red);2010/11 in the upper plot and 2011/12 in the lower plot; upper boundary: air temperature & energy balance

The performance of the model was also tested for temperature simulations of deeper ponds. In Figure 5.2, the result of the simulation of the temperature development for a pond with depth 1.27 m is shown in comparison to measurements from a pond with the same depth (M013). The simulation results for a pond with a depth of 1.21 m in comparison to measured data from pond 'M011' show very similar results and are shown in Figure A.6 in the annex A.2. Results are described exemplarily for pond 'M013'.

The overall performance with an R^2 of 0.76 was better than for the shallow pond with the depth 0.81 m. Winter temperatures were slightly better represented, although the same effect for the two different winters was observed again. Simulations underestimated temperatures at the surface and at 75 cm below the water surface during the winter 10/11 and overestimated them during winter 11/12. Summer temperatures were well simulated at the surface but at 75 cm below the water surface the simulated temperatures did not show the same behaviour as the measured temperatures. The measured temperature profile indicates pronounced mixing of the pond and the water column was nearly isothermal. This mixing was not captured at all times by the simulations. Especially during the summer 2011, when water temperature reached peak temperatures of 23°C

the simulated temperature at 75 cm below the water surface stabilized at ~4°C. The coefficients of determination for simulations of ponds are summarized in Table 5.1.

Table 5.1 Coefficients of determination R^2

Simulation	upper boundary condition	10/11	11/12	10/12
M003 (water surface)	air temperature	0.1049	0.4069	0.3755
M003 without snow (water surface)	air temperature	-1.6537	0.8859	0.3510
M003 (surface at air interface)	air temperature	0.9465	0.9563	0.9510
M011 (water surface)	air temperature	-0.6180	0.8207	0.6677
M013 (10 cm below water surface)	air temperature	0.3844	0.8276	0.7646
M003 (41 cm below water surface) (Results see next chapter)	water surface temperature	0.9303	0.9774	0.9654

5.2. Sensitivity analysis

Effect of snow cover on Water Temperature Simulations

In Figure 5.3 the measured monthly mean water surface temperature is shown in comparison for two different simulations, one with and one without snow cover. Again, simulations during summer fit quite well with the measured temperatures but during the winter months (October-February) and spring-melt and ice break-up during May a large spread is noticable. Measured pond temperatures itself were very different for the winters 10/11 and 11/12. As prevailing air temperatures for both years differed only slightly during winter (cp. Figure A.7 in annex A.6), a sensitivity analysis with respect to snow cover was conducted. Therefore, a comparison of the performance of the model was done for two runs, one including snow cover and the other one without.

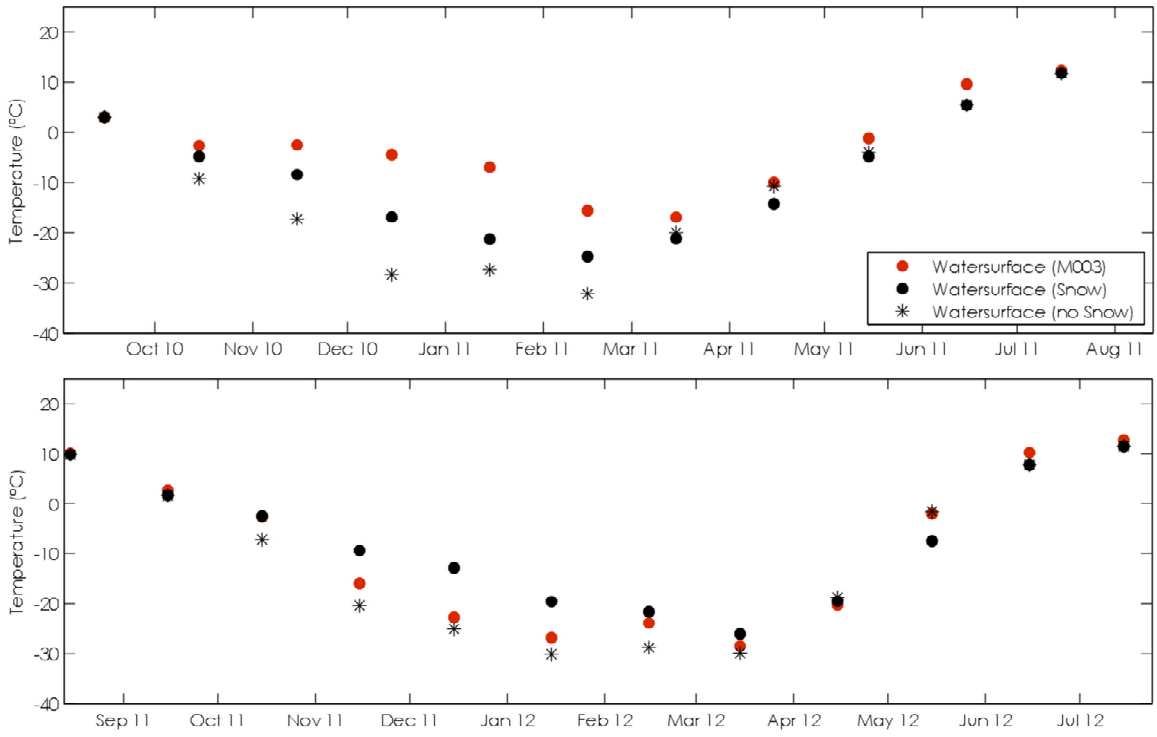

Figure 5.3 Comparison of measured monthly mean temperature (red circle) of pond M003 (depth: 0.81 m), modelled monthly mean temperature with snow cover (black circle) and modelled monthly mean temperature without snow cover (black asterisk);2010/11 (top) 2011/12 (bottom); upper boundary: air temperature & energy balance

Both versions underestimated water temperatures from Oct-Feb 2010 temperatures over the whole profile in 2010/11 significantly. The overall R^2 for the simulation with snow cover was 0.1049 and reached negative values for simulations without snow cover. In contrast, the R^2 for the simulation without snow cover was 0.8859 for the winter 11/12 and 0.4069 for simulations with snow cover. During this period, the simulations without snow cover represented the observed temperature development much better than the one without. The deviations during spring melt were only slightly smaller for simulations without snow cover in the first year but the sudden temperature increase in May 2012 was again captured better by the simulatios without snow cover (cp. also with the lower plot in Figure A.4 in annex A.6).

Surface Energy Balance Forcing

To check the performance of the surface energy balance calculations the comparison of modelled and measured surface temperature (temperatures at the air-water, air-ice or air-snow interface measured with an infrared surface temperature sensor) is shown in Figure 5.4. The simulations reproduced the surface temperatures very well also during winter. Greatest deviations of about 5°C were observed during spring melt in May and June during both years. The coefficient of determination for that time was 0.9510.

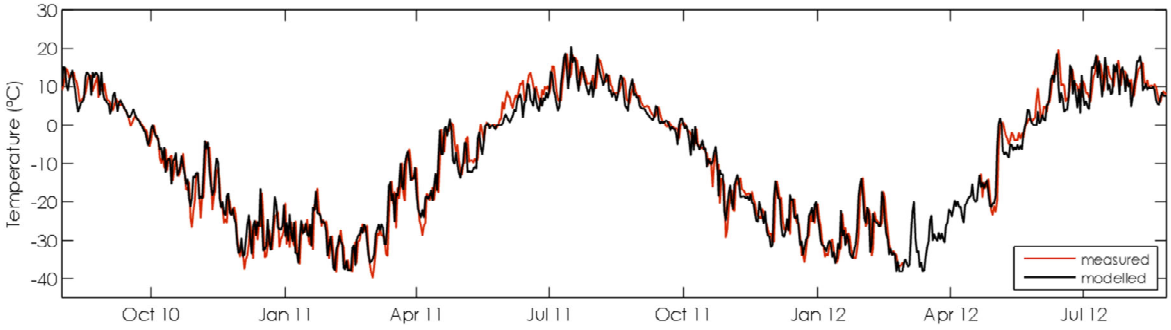

Figure 5.4 Comparison of simulated (black) and measured (red) surface temperature development at the air interface; upper boundary: air temperature & energy balance

Some minor underestimation was observed for sudden low temperatures after preceding warmer temperatures during the winter months November to January.

Water Surface Temperature Forcing

In Figure 5.5, simulation results of a model run using measured water surface temperatures as the upper boundary condition are shown and therefore snow cover and energy balance simulations were excluded from the calculation sheme. In comparison to Figure 5.1, the results are much improved (R^2 = 0.96). Simulated summer temperatures as well as winter temperatures followed the measured temperatures closely. Only minor deviations in summer (1-2°C) and significantly reduced deviations in winter (~5°C) were observed. Simulated temperatures were always above measured temperatures, in contrast to simulations including snow cover and surface energy balance. Maximum deviations at 41 cm below the water surface of 5-7°C occurred during February 2011 and January 2012. The warming of deeper layers was delayed by about two weeks in both years. Simulated temperatures were still affected by phase transition while the measured temperatures were already decreasing. Ice melt was delayed by about one week at 41 cm below the surface.

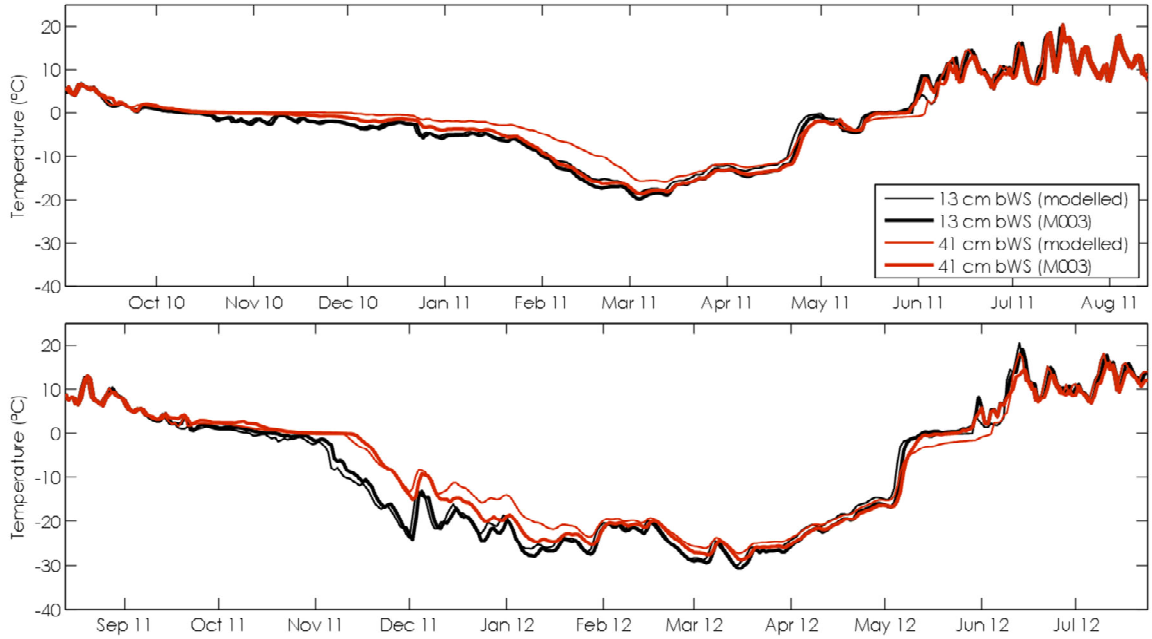

Figure 5.5 Comparison of modelled (thin) and measured (thick;M003) temperatures 13 cm below the water surface (black) and 41 cm below the water surface (red) for a pond with a depth of 81 cm, 2010-2011 (upper figure) and 2011-2012 (lower figure).; upper Boundary: Water Surface Temperature

5.3. Validation for Lake Dry

In Figure 5.6, the results of simulations for a lake with a depth of 3.4 m with air temperature forcing are shown in comparison with the measured data from 'Dry' lake. Certain issues in representing temperature development were noted. Summer temperatures were generally underestimated and too high during winter. During the end of September, measured temperatures decreased isothermally to nearly 0°C. After this minimum the temperatures increased again and stronger at the pond bottom. Simulated temperatures stopped decreasing in the beginning of September at a temperature of ~4°C. Although a slight 'edge' of de- and increasing of simulated temperatures at 2 above the bottom had been noted in the end of September the temperatures at the bottom were affected throughout the winter by the offset gained during September. A gradual decrease of simulated temperatures led to alignment of simulated and measured temperatures in March at 2 m above the lake bottom and in May at the bottom. Measured temperatures rose above 0°C in the beginning of July and simulated temperatures had a delay of about a month before a temperature increase was visible.

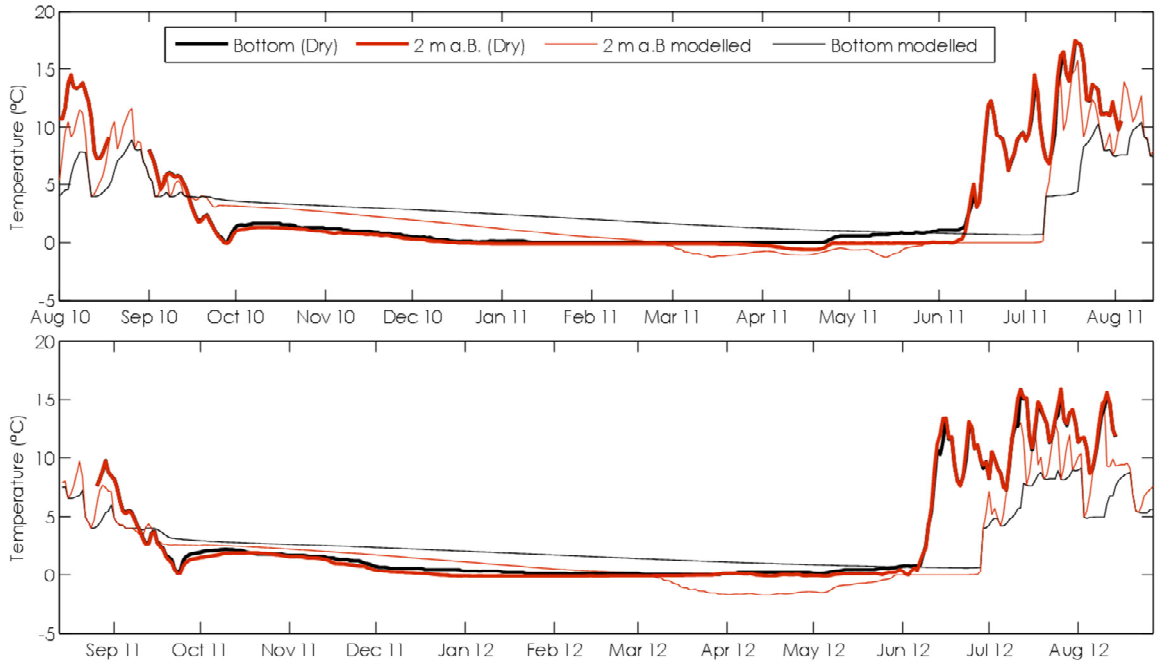

Figure 5.6 Comparison of measured (thick) and modelled (thin) Temperatures at the bottom (black) and 2 metres above (red) of a water body with 3.4 m depth; presented are the years 2010/11 (top) and 2011/12 (bottom)

The modelled water body froze in the beginning of March in both years at a depth of 1.4 m (2 m above Bottom) whereas measured temperatures barely dropped below 0°C in mid-April short before temperatures started to rise again in the end of April.

5.4. Long Term Simulations for Talik development

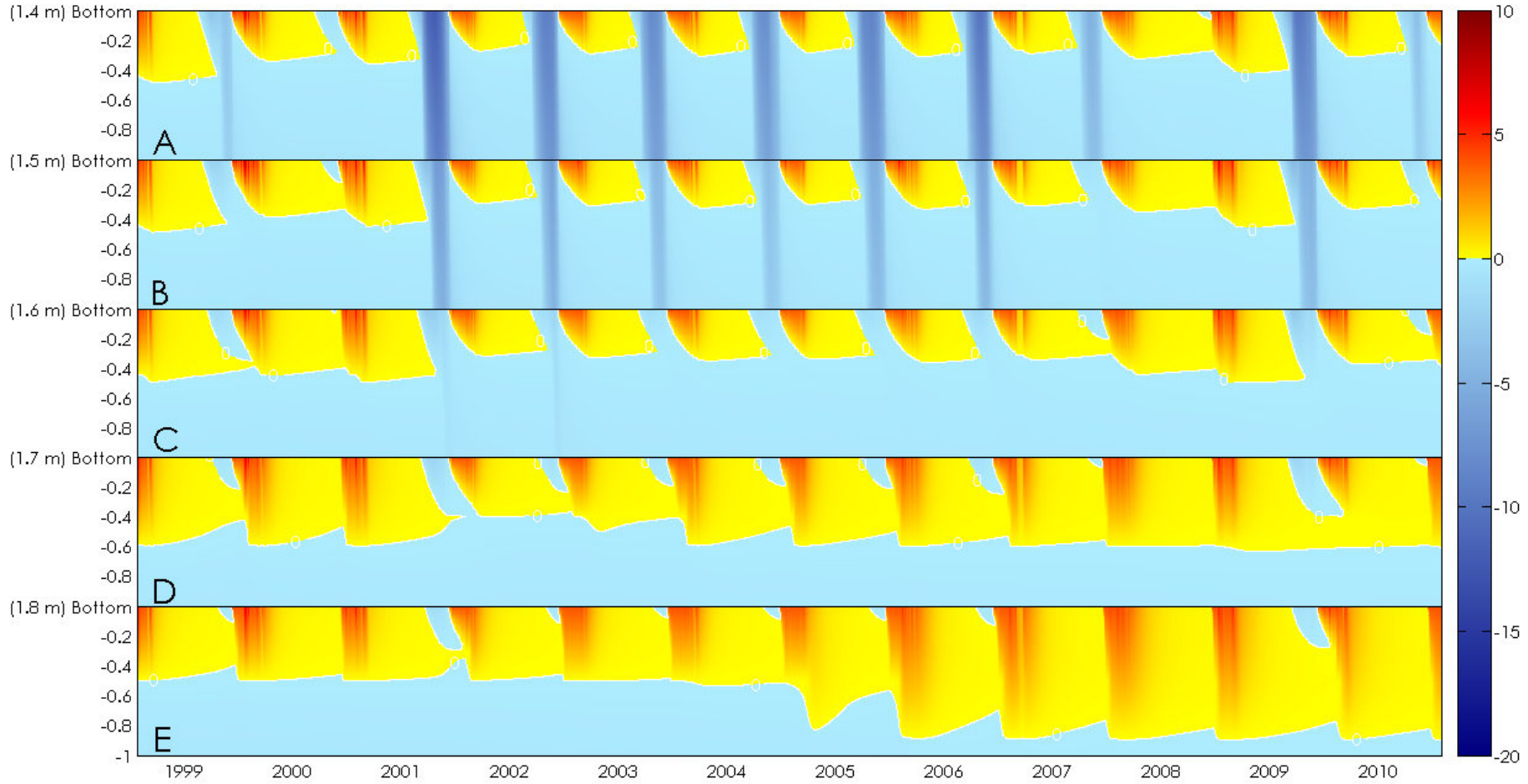

Figure 5.7 Temperature distribution within the first meter of sediment below 5 ponds with increasing depth(A 1.4m; B 1.5 m; C 1.6 m; D 1.7 m; E 1.8 m) from 1998 to 2010

The results of long term simulations with air temperature forcing over 12 years are shown in Figure 5.7. It depicts the temperature distribution within the first meter of sediment below the pond bottom for 5 ponds with increasing depth (1.4-1.8 m). Blue colours indicate sediments with temperatures below 0°C and yellow to red colours indicate sediments with temperatures above 0°C. Maximum thaw depths below the pond bottom ranges annually from 30 cm to 45 cm but did not show significant changes with increasing pond depth up to a depth of 1.6 m. Simulation results for shallower ponds not shown in Figure 5.7 led to the same assumption. Although the thaw depth below the water bodies did not change significantly, the time of completely frozen sediments during winter grew shorter with increasing depth. In the winter 2002/03, the pond with the depth 1.4 m had 95 days with no sediment cell of temperatures above 0°C, the pond with 1.5 m depth only 69 days, 1.6 m 42 days and below a pond with 1.7 m depth there was at all times at least one sediment cell unfrozen. A continuous *talik* was formed and during the consecutive years the thaw depth increased further. Continuously thawed sediments were present at depths ranging from 30 cm to 60 cm below the pond bottom. Maximum thaw depth below a pond with 1.8 m water depth was simulated to be 85 cm. The frost table underneath the *talik* was not stable at one depth but froze back during winter by about 10 cm for the years 2006 to 2010 to depths of 0.6 to 0.7 m below the pond bottom.

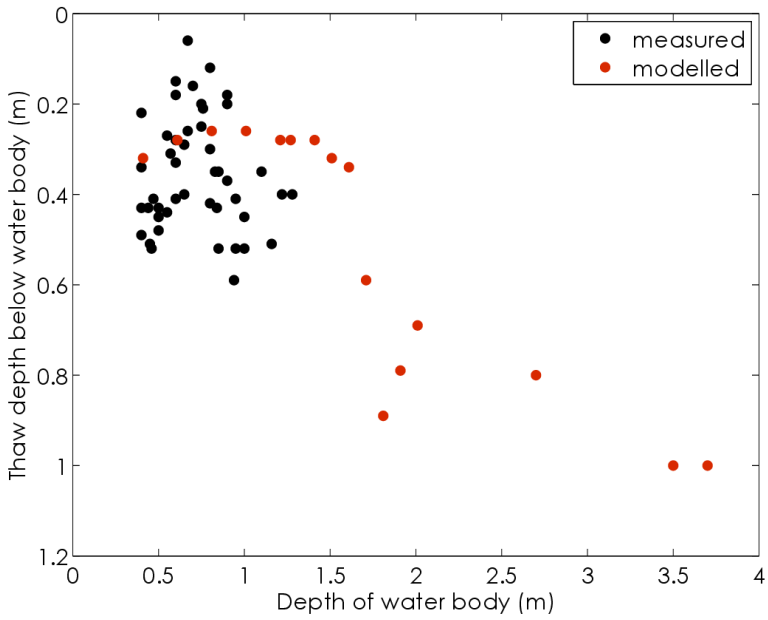

Figure 5.8 Simulation results for maximum thaw depth in 2003 (red) and thaw depth measurements (black) in Aug 2011 [*Wischnewski*, 2012] below a water body versus the depth of the water body

Figure 5.8 shows the simulated maximum thaw depth below ponds in relation to water body depth for simulations in August 2003 and measurements of thaw depth during August 2011. Simulation results show that water bodies with depths below 1.7 m had a maximum thaw depth ranging from 26 to 34 cm. Water bodies deeper than that showed considerably increasing maximum thaw depths. Thaw depth measurements were only available for depths up to 1.3 m and show a large spread between a few centimetres up to 60 cm thaw depth below the water body. Absolute values (water depth + thaw depth) for maximum thaw depth above 3 m only give indications on thaw depth, as spatial discretisation is becoming coarse. This is the reason for decreasing maximum thaw depth between 1.7 m and 2 m water body depth.

5.5. Effect of temperature increase on talik development

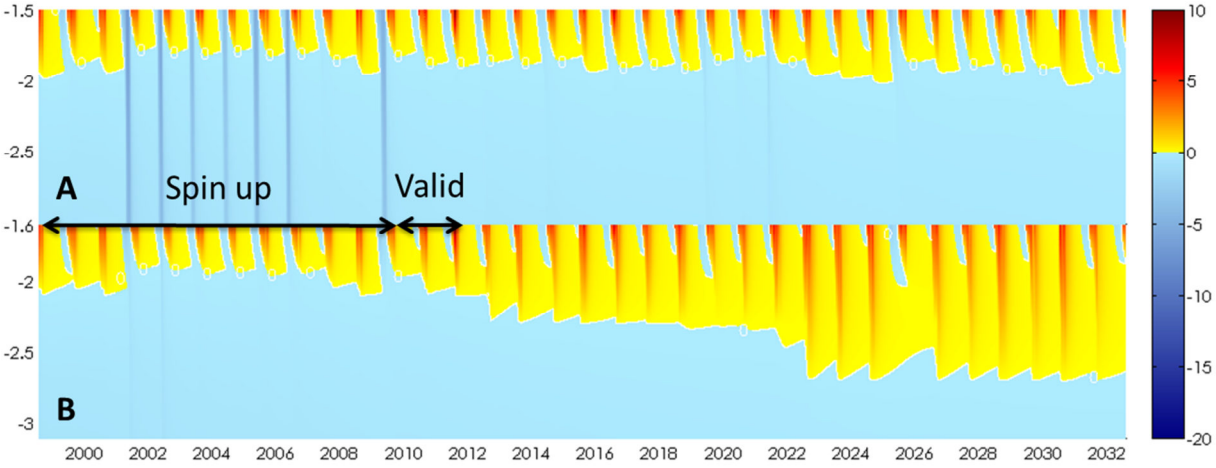

Figure 5.9 *Talik* development under the influence of temperature increase of 0.1°C per year starting in 2012 for a water body with depth A) 1.5 m and B) 1.6 m; depicted is 1.5 m of sediments below the water body

In Figure 5.9, the response of *talik* development to an increase of air temperatures (0.1°C per year) is shown. From 1998 to 2012, measured air temperatures were used as boundary conditions and gradual increase of air temperature started in 2012 for 20 years until 2032. Both water bodies (Figure 5.9 A) depths: 1.5 m; B) depth: 1.6 m) were not developing a continuous *talik* within the years 1998 to 2010 (cp. results in chapter 5.4). The shallower pond (Figure 5.9 A) did develop a *talik* only for singular years until 2032. However, the maximum thaw depth increased from 30 cm in 2003 to about 50 cm in 2032. In the case of the 10 cm deeper pond (Figure 5.9 B), a *talik* developed already during the validation period from 2010 to 2012 and deepened in the following summer by about ~20°cm and again in 2022, where the *talik* was deepened by further 60 cm. The effect of coarse grid cells explained in the previous chapter can be observed in Figure 5.9 again and the increase of thawed sediments below the sediment did not increase necessarily as sudden as indicated by the simulations but could have also happened more gradual.

6. Discussion

The aim of this study was to develop a model capable of simulating temperature development within the water column and underlying sediments of small water bodies in the Arctic polygonal tundra.

6.1. Model Assessment

The simulation results showed good accordance with measured data during summer months (June-September) and the second half of the winter (mid-March to April). Significant deviations were observed during early winter (October-February) and during ice break-up (May), which led to an overall low coefficient of determination.

To rule out significant errors originating from surface processes such as energy balance or absorption of short wave radiation, the simulated surface temperature was compared to the measured surface temperature (Figure 5.4). As cells at the air interface were represented well in the model and temperature deviations started to increase as soon as snow cover was building up it was assumed that errors originated from snow cover parameterisation or input snow depth.

Winter temperatures in ponds

One error source related to snow cover is certainly the assumption of constant snow parameters throughout the simulation. As already pointed out before, settled snow undergoes compaction processes over time, which has implications on the snow density [*Sturm and Holmgren*, 1998]. The deviations in early winter simulation results could originate from an inappropriate choice of thermal conductivity for this period as it is very low in fresh snow and only increases with time when snow becomes denser [*Mellor*, 1976; *Riche and Schneebeli*, 2013; *Sturm et al.*, 1997]. In early winter months, effects of wrong representation of snow cover may have a strong impact on temperatures below the snow pack. The temperature gradient during this period is comparably large because air temperatures are already below 0°C whereas water temperatures are still well above 0°C (cp. Figure A.5). In this case, an overestimation of thermal conductivity of the snow layer leads to an overestimated cooling of the water column. The same is true for the melting season when air temperatures are increasing from well below 0°C to about 10°C in a matter of days. Hence, the heat fluxes into the ground during this period will be large. High insulation resulting from a thick snow cover will keep temperatures stable below the snow and keep the pond from cooling down or heating up respectively. In the opposite case, if snow cover is very thin or not present at all, heat can be transported unhindered in or out of the ground and temperatures will show similar gradients as air temperatures.

Besides parameterisation but the input data itself could be a source of error. Comparisons with onsite photographs of the area surrounding the meteorological station show that especially during the end of the snow cover season measurements from the sonic ranging sensor were flawed. The photographs show that in spring the snow was completely melted until the end of May; 1 month earlier than measurements indicated (cp. Figure A.8 in annex A.6). In fact snow depth measurements experienced a peak during June, which might be due to pooling water on the site where snow depth is measured or due to other disturbances like vegetation growth. Both years also

experienced an earlier melt event at the end of April which nearly removed all the snow. After a few days snow fall led to a build-up of snow cover on the ground again. Measured temperatures at the water surface of the ponds indicate that this short period without snow cover was enough to raise temperatures of the entire water column up to 0°C. As measured input snow cover was never removed completely during April, the simulated temperatures could not increase as well because the conduction of heat was hindered. This was also confirmed by results of simulations without snow cover, where the temperature development is representing measured temperatures much better during May (cp. Figure A.4). The 'falsely measured' snow cover during June does not seem to pose a problem. During that period measured snow depth now and then drops to zero and if only once the upper most cell reaches a temperature above 0°C no snow cover will be simulated anymore due to the implemented condition of a frozen surface.

Results indicate that not only the timing but also the magnitude of snow depth over the entire period might have been different in comparison to the snow depth at the measuring site of the snow sensor. An underestimation of snow depth leads to a reduced insulation of the ground [*Grundstein et al.*, 2005] and might be an explanation for the large deviations of simulated temperatures from measured values during the year 2010/11 in the validation period. The sonic ranging sensor measures snow depth over a polygon centre, which is not filled with water and represents only a point measurement. Snow is not homogeneously distributed due to wind drift and the interacting pronounced micro topography [*Essery and Pomeroy*, 2004]; therefore errors for measurements at a specific location are to be expected. As pointed out before, start and end of the cold season are critical for temperature development in the ground. Therefore, the time of occurrence and end of snow cover being wrongly implemented has implications on the modelled outcome.

Despite the large deviations between measured and simulated early winter temperatures, the differences decreased as soon as air temperatures start to rise until end of April. This might be due to the fact that air temperatures drop to around -30°C very quickly in the beginning of winter and then fluctuate around this temperature until mid-April. During this time, the temperature difference in the simulated scenario is smaller than in the measurements. This difference leads to further decreasing measured temperatures and a more or less stable temperature in the modelled case; leading to decreasing differences of measured and modelled temperatures. Due to generally smaller temperature gradients from the end of March to the end of April the influence of snow cover becomes less important, hence deviations do not increase further.

The large deviations due to snow cover made it difficult to disentangle possible other error sources. For that reason, a further simulation was conducted with *water surface temperatures* as the upper boundary condition, replacing surface energy balance and air temperature. In this scenario temperatures below the snow pack are known, hence no simulation of snow cover needed to be conducted. As expected, the modelled temperatures showed a much better fit than before. R^2 values for water temperatures below the water surface for the entire year increased from 0.35 to 0.96. Maximum deviations were again observed during winter but did not increase before the end of January in both years. In this simulation winter temperatures were underestimated. As deviations amplified with increasing ice thickness the thermal conductivity of ice was assumed to be underestimated. The effect of stronger gradients resulting in a larger absolute error as before for the snow parameterisation might also enhance deviation

during that period. The model uses constant values for the thermal conductivity of ice. But thermal conductivity of ice is dependent on temperature and the value chosen is a typical value for ice at about -10°C and thermal conductivity increases with decreasing temperatures [*Powell*, 1958].

Another reason for temperature deviations between measured and simulated data might be the fact that the measurement sensor position is not exact. Sensors are attached by a rope to an anchored buoy giving the entire temperature chain moderate room for movement. Due to the strong temperature gradient between surface and bottom of ice only minor shifts in height might implicate major shifts in temperature. During ice melt slight deviations from measured temperatures were observed. Simulated temperatures were affected by phase change processes (zero curtain) than measured temperatures. This was possibly due to the fact, that short wave radiation is absorbed only in the upper most material, assuming that no light is penetrating through the ice into the water (the case in autumn). For most of the time when ice is covering the water surface no short wave radiation is present due to polar night, but in spring the sun comes back and the ice layer starts to melt. In the modelled case, there are a few cells thawed on top and the rest is still frozen but the model scheme is only absorbing radiation in those uppermost cells. During this time the assumption of only one material being penetrated by light might not be accurate enough, as radiation is likely to pass through the water layer into the ice and inserts energy into those cells as well. Neglecting the penetration of light may lead to a delay in thawing of the ice cover.

Summer temperatures in ponds

Although snow cover had the largest impact on the quality of the simulation results other error sources might have led to deviations from measured temperatures. During summer the dominant process affecting observed temperature profiles was wind mixing, which led to a nearly isothermal temperature regime within the water column [*Wischnewski*, 2012]. This was in general represented well by the model, but in cases of slightly deeper water bodies mixing did not reach the bottom of the water body and measured temperatures of deeper water layers tended to be underestimated by the model. There are two parameters mainly influencing the efficiency of mixing in the model. The first is the magnitude of the calculated turbulent kinetic energy (TKE), which determines the depth of entrainment or the thickness of the mixed layer. Owing to high values for TKE, entrainment usually reached also the lowest water cell in the model. This deep entrainment indicates that the choice of ω from equation (10) might have been too low. However, this factor was chosen quite high in comparison to published values [*Hondzo and Stefan*, 1993] but results show that warm air temperatures were still not transported efficiently enough to deeper layers.

General underestimation of summer temperatures in the water column might also originate from simplifications of the calculation scheme of the surface energy balance. Aerodynamic resistance influences sensible and latent heat fluxes both, and its calculation is based on the assumption of neutral atmospheric conditions. Those conditions frequently occur during summer months on Samoylov [*Langer et al.*, 2011b] but when the conditions are not fulfilled corrections for stability need to be included and omission can lead to wrong estimates for the turbulent fluxes. The surface energy balance is a complex mechanism described by a large number of parameterisations of emissivity and albedo for different surface materials and combined errors might enhance

each other and result in an amplification of errors. Another simplification is the calculation of fluxes with surface temperatures calculated from the time step before and this should correctly be implemented as a process of mutual interaction as the magnitude of turbulent fluxes is influencing the surface temperature and vice versa.

Temperature simulation in lakes

What has already been observed for deeper ponds is very obvious in the lake simulation. The transport of heat to deeper water layers was not as efficient in the modelled case as it is in the measured temperature data. Although modelled entrainment reached the lowest water cell most of the time, warm temperatures did not. This discrepancy can either be due to too low hypolimnetic eddy diffusivity K_z or due to the fact that density driven stratification is overriding the effect of wind mixing. As modelled temperatures often stagnated at the temperature of the highest density of water (~4°C) the latter is thought to be the dominant reason. If so, this is even enhanced by the direct dependence of the magnitude of hypolimnetic eddy diffusion on the stability of the water column. Consequently, the more stable the water column is, the less influential wind induced mixing becomes. As it is implemented in the model, the water column in simulations is at all times stable (Brunt-Vaisala frequency $N^2>0$) because sorting of cells according to density is done at every time step, and theoretically a cell warmed up to 4°C at the water surface could be 'transported' to the very bottom within one single time step if no heavier cells are in between. This immediate transport is a rather crude assumption and leads to acceleration of the stratification process. This effect might not have had such a large impact on the simulation results for the shallower water bodies, as maximum 'transport distance' is constrained by the shallow depth. In order to achieve a better representation of the slow descent of water cells with a higher density a time lag would need to be implemented to slow down the process. This could be accomplished by defining certain 'maximum shift distances' for the single cells so as to prevent the case described above.

In autumn when measured temperatures started to decrease to 0°C at the end of September the simulated temperatures stagnated again at ~4°C. This offset is then influencing the simulated temperature development throughout the entire winter. Ice thickness was slightly overestimated but the deviations to measured results could also originate from the issue mentioned before of free moving measurement sensors on a temperature chain, which might have an even greater effect in the deeper lakes. The great delay of about 1 month of rising temperatures in spring can be explained by the delayed removal of snow cover due to faulty measurement data. In the case of the shallow ponds the ice-melt results in pooling water on top of the remaining frozen water cells which are not uplifted as they are still frozen to the ground. As explained before this prevented snow to build up again on the ponds although measurements still indicated a certain snow depth. In the case of a deep lake, where the ice is floating at all times snow cover cannot be removed until the entire ice has been melted, hence a delay of ice cover break-up was the result. Another short delay of about a week might have been introduced by the implemented wind mixing scheme, which was programmed not to start until the surface reaches temperatures of at least 0.5°C.

6.2. Talik development

Long term simulations over 12 years were carried out in order to inspect the temperature development of the sediment below water bodies with varying water depth. Although the magnitude of temperature dynamics might not be exact due to reasons mentioned above, it was still possible to identify certain behaviours related to *talik* development. Results were analysed in respect to maximum thaw depth below the water body and duration of thawed versus frozen states within the sediments. Annual changes in maximum thaw depth below water bodies with invariable depth were observed. Water bodies shallower than 1.6 m developed maximum thaw depths ranging from 30 to 45 cm. However, comparing the maximum thaw depth for a single year below water bodies with changing depths, the simulation results suggested that no significant increase of thaw depth was caused by increasing water depth. Instead the total time of completely frozen sediments below the water body changed with increasing water depth (+10 cm). The time of the thawed state grew shorter by about 1 month as it took longer for the cold to penetrate to deeper layers in autumn. The beginning of thaw in spring did not change significantly. This behaviour implies that *talik* development is mainly influenced by processes during the winter. Due to high thermal conductivity and effective wind mix in the water column, heat is quickly transported to the underlying sediments soon after the ice cover is removed. In contrast, extracting heat during the winter takes considerably longer, as conduction through ice and snow is slowed down. When snow cover is very thick or winter temperatures are mild a stable condition of annually refreezing sediments below the water body can be disrupted. The sediments may not freeze back and maximum thaw depth increases during the following summer and ultimately a *talik* may develop. On the other hand, if a winter is very cold and temperatures penetrate deep into the ground a *talik* could cease to exist and creates a relapse of the thermal regime within the sediments underlying the water would be created.

In the simulations, a continuous *talik* developed under a water body with a depth of 1.7 m in the period from 1998 to 2010. With increasing water depth maximum thaw depth further increased as well. This result implicates that once a *talik* has formed water depth influences maximum thaw depth. Simulations for deeper lakes could only be interpreted in a very general sense as spatial discretisation grew rather coarse (>20 cm) in the regions below the lake bottom and changes in thaw depth was happening 'step like' at the point when energy was sufficient to thaw a comparably large cell. For detailed information on a more natural development in deeper layers the spatial discretisation would need to be increased. But nevertheless also the results from simulations with an artificial temperature increase of 0.1°C per year resulted in a general increase of thaw depth below water bodies. Results also demonstrated how talik appearance can be triggered by the succession of short term events such as mild winters or a very thick snow cover succeeded by a warm summer rather than by long term air temperature increase.

7. Summary and Conclusion

The aim of this thesis was to design a model capable of simulating temperatures of arctic ponds and the underlying sediments. The resulting model was based on a one dimensional model for heat transport in soils with the ability to calculate phase change. Adaptions were made to include processes influencing heat transport in water bodies, such as density driven stratification, wind induced mixing and absorption of light within the water column. The model was forced with meteorological data such as air temperature, humidity, atmospheric pressure, wind speed and snow depth. Surface energy balance calculations were also included to the modelling scheme.

- The model was capable to capture basic features which dominate the thermal dynamics of Arctic ponds such as a predominating advective heat transport during summer and conductive transport in winter. General behaviour like the zero curtain in spring and autumn and fast warming of the water column during summer was represented well and has been validated with measurements. Simulations for deeper lakes showed shortcomings with respect to density driven advection. In comparison to measurements the density driven advection was too strong and diminished wind induced mixing significantly. In order to solve this problem for future applications it is recommended to introduce a mechanism that prevents water cells with higher density from being shifted too quickly to lower layers in the water column.
- Shortcomings with respect to the parameterisation of the snow cover were identified. It has been shown that snow cover is the most critical factor for modelling winter temperatures. Hence, it is strongly recommended to include a more sophisticated snow scheme which is capable to account for changing thermal properties of snow with time. Snow depth input data has to be verified or calibrated.
- Long term simulations of the thermal regime below water bodies with different depths showed that there is a threshold behaviour in respect to development of continuously thawed sediments below water bodies (*talik*). For shallow ponds the maximum thaw depth within the bottom sediments was observed to be stable until a certain water depth. Once this critical depth was reached, the thaw depth started to increase. Although simulation results may not be exact in terms of magnitude of temperature and timing, it has been shown that only a change of about 20 cm in water body depth led to a rapid *talik* development.
- Under the assumption of warming air temperatures by 0.1°C per year a general deepening of the thaw depth below the water bodies was observed. In this scenario *talik* development was observed under ponds with a lower depth. However, the results of the simulations indicate that *talik* development is rather triggered by the succession of single events like a mild winter or a thick snow cover which increased thaw depth below the water body and led to *talik* development. With continuing increase of the thaw depth even colder winter temperatures are needed to freeze back underlying sediments.

Concluding it can be said the results of this thesis identified important processes for modelling arctic ponds. Due to the large number of appearance of small water bodies in Arctic tundra environments an improved version of the model can be an asset for the analysis of the susceptibility of permafrost overlain by shallow water bodies.

References

Abnizova, A., J. Siemens, M. Langer, and J. Boike (2012), Small ponds with major impact: The relevance of ponds and lakes in permafrost landscapes to carbon dioxide emissions, *Global Biogeochem. Cycles*, *26*(2), GB2041.

ACIA (2004), Impacts of a Warming Arctic: Arctic Climate Impact Assessment*Rep.*

Alduchov, O. A., and R. E. Eskridge (1996), Improved Magnus form approximation of saturation vapor pressure, *J. Appl. Meteorol.*, *35*(4), 601-609.

AMAP (2011), Snow, Water, Ice and Permafrost in the Arctic (SWIPA): Climate Change and the Cryosphere*Rep.*, xii + 538 pp pp, Arctic Monitoring and Assessment Programme (AMAP), Oslo, Norway.

Boike, J., M. Langer, H. Lantuit, S. Muster, K. Roth, T. Sachs, P. Overduin, S. Westermann, and A. D. McGuire (2012a), Permafrost – Physical Aspects, Carbon Cycling, Databases and Uncertainties, in *Recarbonization of the Biosphere: Ecosystems and the Global Carbon Cycle*, edited by R. Lal, pp. 159-185, Springer Science+Business Media.

Boike, J., B. Kattenstroth, K. Abramova, N. Bornemann, A. Chetverova, I. Fedorova, K. Fröb, M. Grigoriev, M. Grüber, and L. Kutzbach (2012b), Baseline characteristics of climate, permafrost, and land cover from a new permafrost observatory in the Lena River Delta, Siberia (1998– 2011), *Biogeosci. Disc.*, *9*(10), 13627.

Brown, J., O. Ferrians Jr, J. Heginbottom, and E. Melnikov (1997), Circum-Arctic map of permafrost and ground-ice conditions. USGS Circum-Pacific Map Series CP-45.

Campbell, G., J. Jungbauer Jr, W. Bidlake, and R. Hungerford (1994), Predicting the effect of temperature on soil thermal conductivity, *Soil Sci.*, *158*(5), 307-313.

Cathcart, T. P., and F. W. Wheaton (1987), Modeling temperature distribution in freshwater ponds, *Aquacult. Eng.*, *6*(4), 237-257.

De Vries, D. A. (1966), Thermal Properties of Soils, in *Physics of Plant Environment*, edited by W. R. Van Wijk, pp. 210-235, Amsterdam.

Endrizzi, S., W. Quinton, and P. Marsh (2011), Modelling the spatial pattern of ground thaw in a small basin in the arctic tundra, *The Cryosphere Discussions*, *5*, 367-400.

Essery, R., and J. Pomeroy (2004), Vegetation and topographic control of wind-blown snow distributions in distributed and aggregated simulations for an Arctic tundra basin, *Journal of Hydrometeorology*, *5*(5), 735-744.

Ford, D. E., and H. G. Stefan (1980), Thermal predictions using integral energy model, *Journal of the Hydraulics Division*, *106*(1), 39-55.

French, H. (2007), *The periglacial environment*, Wiley.

Fröb, K. (2011), Measuring and modeling of soil thermal properties and ground heat flux at two different sites at Lena Delta, Siberia, 61 pp, Universität Leipzig.

Garratt, J. R. (1994), *The atmospheric boundary layer*, Cambridge university press.

Goodrich, L. E. (1982), The Influence of Snow Cover on the Ground Thermal Regime, *Candian Geotechnical Journal*, *19*, 421-432.

Grigoriev, N. (1960), The temperature of permafrost in the Lena delta basin–deposit conditions and properties of the permafrost in Yakutia, *Yakutsk*, *2*, 97-101.

Grundstein, A., P. Todhunter, and T. Mote (2005), Snowpack control over the thermal offset of air and soil temperatures in eastern North Dakota, *Geophys. Res. Lett.*, *32*(8), L08503.

Gu, R., and H. G. Stefan (1990), Year-round temperature simulation of cold climate lakes, *Cold Regions Science and Technology*, *18*(2), 147-160.

Hillel, D. (1982), *Introduction to soil physics*, Academic press New York.

Hondzo, M., and H. G. Stefan (1993), Lake water temperature simulation model, *J. Hydraul. Eng.*, *119*(11), 1251-1273.

Jeffries, M. O., T. Zhang, K. Frey, and N. Kozlenko (1999), Estimating Late-Winter Heat Flow to the Atmosphere from the Lake-Dominated Alaskan North Slope, *Journal Glaciology*, *45*, 315-347.

Johansen, Ø. (1975), Thermal conductivity of soils, Ph.D thesis, Available as USACRREL Draft Transl. 637, 1977 pp, Trondheim, Norway.

Jorgenson, M. T., Y. L. Shur, and E. R. Pullman (2006), Abrupt increase in permafrost degradation in Arctic Alaska, *Geophys. Res. Lett.*, *33*(L02503), doi:10.1029/2005GL024960.

Kell, G. S. (1975), Density, thermal expansivity, and compressibility of liquid water from 0. deg. to 150. deg.. correlations and tables for atmospheric pressure and saturation reviewed and expressed on 1968 temperature scale, *J. Chem. Eng. Data*, *20*(1), 97-105.

Lachenbruch, A. H. (1962), *Mechanics of Thermal Contraction Cracks and Ice-Wedge Polygons in Permafrost*, New York.

Langer, M., S. Westermann, S. Muster, K. Piel, and J. Boike (2011a), The surface energy balance of a polygonal tundra site in northern Siberia–Part 2: Winter, *The Cryosphere*, *5*, 509-524.

Langer, M., S. Westermann, S. Muster, K. Piel, and J. Boike (2011b), The surface energy balance of a polygonal tundra site in northern Siberia–Part 1: Spring to fall, *The Cryosphere*, *5*, 151-171.

Langer, M., S. Westermann, M. Heikenfeld, W. Dorn, and D. J. Boike (2013), Satellite-based modeling of permafrost temperatures in a tundra lowland landscape, *Remote Sensing of Environment, in review*.

Lashof, D. A., and D. R. Ahuja (1990), Relative contributions of greenhouse gas emissions to global warming.

Lide, D. R. (2012), *CRC handbook of chemistry and physics*, CRC press.

Lin, Z., F. Niu, Z. Xu, J. Xu, and P. Wang (2010), Thermal regime of a thermokarst lake and its influence on permafrost, Beiluhe Basin, Qinghai Tibet Plateau, *Permafr. Periglac. Proc.*, *21*, 315-324.

Luojus, K., J. Pulliainen, M. Takala, C. Derksen, H. Rott, T. Nagler, R. Solberg, A. Wiesmann, S. Metsamaki, and E. Malnes (2010), Investigating the feasibility of the

GlobSnow snow water equivalent data for climate research purposes, paper presented at Geoscience and Remote Sensing Symposium (IGARSS), 2010 IEEE International, IEEE.

McGuire, A. D., L. G. Anderson, T. R. Christensen, S. Dallimore, L. Guo, D. J. Hayes, M. Heimann, T. D. Lorenson, R. W. Macdonald, and N. Roulet (2009), Sensitivity of the Carbon Cycle in the Arctic to Climate Change, *Ecol. Monogr.*, *79*(4), 523-555.

Mellor, M. (1976), Engineering properties of snow, paper presented at Symposium on Applied Glaciology.

Mironov, D. V. (2008), Parameterization of lakes in numerical weather prediction. Description of a lake model*Rep.*, COSMO technical report.

Mooney, P., F. Mulligan, and R. Fealy (2011), Comparison of ERA-40, ERA-Interim and NCEP/NCAR reanalysis data with observed surface air temperatures over Ireland, *Int. J. Climatol.*, *31*(4), 545-557.

Muster, S., M. Langer, B. Heim, S. Westermann, and J. Boike (2012), Subpixel heterogeneity of ice-wedge polygonal tundra: a multi-scale analysis of land cover and evapotranspiration in the Lena River Delta, Siberia, *Tellus B*, *64*.

NASA (2000), NASA Landsat Program, Lena Delta in Landsat 7/ETM+, Visible Earth, v1 ID: 407 18024, edited, pp. Lena Delta, in Landsat 7/ETM+, Visible Earth, v1 ID: 407 18024, USGS EROS Data Center Satellite Systems Branch.

Plug, L. J., and J. J. West (2009), Thaw lake expansion in a two-dimensional coupled model of heat transfer, thaw subsidence, and mass movement, *J. Geophys. Res.*, *114*(F01002), doi:10.1029/2006JF000740.

Powell, R. (1958), Thermal conductivities and expansion coefficients of water and ice, *Advances in physics*, *7*(26), 276-297.

Pulliainen, J. (2006), Mapping of snow water equivalent and snow depth in boreal and sub-arctic zones by assimilating space-borne microwave radiometer data and ground-based observations, *Remote sensing of Environment*, *101*(2), 257-269.

Riche, F., and M. Schneebeli (2013), Thermal conductivity of snow measured by three independent methods and anisotropy considerations, *The Cryosphere*, *7*, 217-227.

Riley, M. J., and H. G. Stefan (1987), *Dynamic lake water quality simulation model" MINLAKE"*, St. Anthony Falls Hydraulic Laboratory, University of Minnesota.

Riley, M. J., and H. G. Stefan (1988), MINLAKE: A dynamic lake water quality simulation model, *Ecol. Model.*, *43*(3), 155-182.

Schwamborn, G., V. Rachold, and M. N. Grigoriev (2002), Late Quaternary sedimentation history of the Lena Delta, *Quat. Int.*, *89*(1), 119-134.

Screen, J. A., and I. Simmonds (2011), Erroneous Arctic temperature trends in the ERA-40 reanalysis: a closer look, *Journal of Climate*, *24*(10), 2620-2627.

Sophocleous, M. (1979), Analysis of water and heat flow in unsaturated-saturated porous media, *Water Resour. Res.*, *15*(5), 1195-1206.

Sturm, M., and J. Holmgren (1998), Differences in Compaction Behaviour of Three Climate Classes of Snow, *Ann. Glaciology*, *26*, 125-130.

Sturm, M., J. Holmgren, M. Koenig, and K. Morris (1997), The Thermal Conductivity of Seasonal Snow, *Journal Glaciology*, *43*(143), 26-41.

Takala, M., K. Luojus, J. Pulliainen, C. Derksen, J. Lemmetyinen, J.-P. Kärnä, J. Koskinen, and B. Bojkov (2011), Estimating northern hemisphere snow water equivalent for climate research through assimilation of space-borne radiometer data and ground-based measurements, *Remote Sensing of Environment*, *115*(12), 3517-3529.

Tipler, P. (1991), Physics for scientists and engineers: mechanics, *WH Freeman*.

Tranvik, L. J., et al. (2009), Lakes and reservoirs as regulators of carbon cycling and climate, *Limnol. Oceanogr.*, *54*(6), 2298-2314.

Van Bavel, C., and D. Hillel (1976), Calculating potential and actual evaporation from a bare soil surface by simulation of concurrent flow of water and heat, *Agr. Meteorol.*, *17*(6), 453-476.

van Everdingen, R. (1998), Multi-Language Glossary of Permafrost and Related Ground-Ice Terms, revised May 2005, *National Snow and Ice Data Center/World Data Center for Glaciology, Boulder, CO*.

Wischnewski, K. (2012), Bathymetric features and thermal dynamics of small ponds and lakes in the arctic tundra, Lena Delta (Siberia, Russia), Project report thesis, 30 pp, Swiss Federal Institute of Technology.

Yershov, E. D., and P. J. Williams (1998), *General geocryology*, Cambridge Univ Press.

A Supplementary Material

A.1. Definitions and Constants

Table A.1 Definitions and constants with corresponding values used within context

A	Empirical constant for freeze curve	19[a]	
A_s	Surface area		m^2
B	Empirical constant for freeze curve	4[a]	
C_a	Specific heat capacity of dry air	1003.5	$J\ kg^{-1}\ K^{-1}$
C_{app}	Apparent heat capacity		$J\ m^{-3}\ K^{-1}$
C_h	Heat capacity		$J\ m^{-3}\ K^{-1}$
C_i	Specific heat capacity of ice at 0°C	2050[b]	$kJ\ m^{-3}\ K^{-1}$
C_m	Specific heat capacity of minerals	2000[c]	$kJ\ m^{-3}\ K^{-1}$
C_o	Specific heat capacity of organic material	2500[d]	$kJ\ m^{-3}\ K^{-1}$
C_w	Specific heat capacity of water	4186[2]	$kJ\ m^{-3}\ K^{-1}$
C_s	Specific heat capacity of snow		$kJ\ m^{-3}\ K^{-1}$
E_{fus}	Energy related to phase change		$W\ m^{-3}$
K_z	Hypolimnetic eddy diffusivity		$m^2\ s^{-1}$
L_v	Latent heat of fusion	334	$kJ\ kg^{-1}$
N^2	Brunt-Vaisala frequency		s^{-1}
Q_E	Latent heat flux		$W\ m^{-2}$
Q_G	Ground heat flux		$W\ m^{-2}$
Q_H	Sensible heat flux		$W\ m^{-2}$
Q_{net}	Net radiation		$W\ m^{-2}$
RH	Humidity		
T	Temperature		K
T_m	Temperature at measuring height		K
T_{surf}	Surface temperature		K
TKE	Turbulent kinetic energy		J
V	Volume		m^3
W_L	Entrainment work		J
f_h	Shape factor (spherical)	1/3[d]	
k_h	Thermal conductivity		$W\ m^{-2}\ K^{-1}$
k_i	Thermal conductivity of ice	2.2[e]	$W\ m^{-2}\ K^{-1}$
k_m	Thermal conductivity of minerals	2.9[f]	$W\ m^{-2}\ K^{-1}$
k_o	Thermal conductivity of organic	0.25[e]	$W\ m^{-2}\ K^{-1}$

[a] Langer, M., S. Westermann, S. Muster, K. Piel, and J. Boike (2011a), The surface energy balance of a polygonal tundra site in northern Siberia–Part 2: Winter, *The Cryosphere*, *5*, 509-524.
[b] Tipler, P. (1991), Physics for scientists and engineers: mechanics, *WH Freeman*.
[c] Yershov, E. D., and P. J. Williams (1998), *General geocryology*, Cambridge Univ Press.
[d] De Vries, D. A. (1966), Thermal Properties of Soils, in *Physics of Plant Environment*, edited by W. R. Van Wijk, pp. 210-235, Amsterdam.
[e] Powell, R. (1958), Thermal conductivities and expansion coefficients of water and ice, *Advances in physics*, *7*(26), 276-297.
[f] Hillel, D. (1982), *Introduction to soil physics*, Academic press New York.

	material		
k_w	Thermal conductivity of water	0.57[e]	W m^{-2} K^{-1}
k_s	Thermal conductivity of snow	0.2[g]	W m^{-2} K^{-1}
a_0		999.83952 e^{-3}	
a_1		169.45176 e^{-4}	
a_2		798.70401 e^{-8}	
a_3		461.70461 e^{-10}	
a_4		105.56302 e^{-12}	
a_5		285.4253 e^{-16}	
b		168.7985 e^{-4}	
g	acceleration of gravity	9.81	m s^{-2}
r_a	aerodynamic resistance		s m^{-1}
t	Time		s
u^*	Shear velocity		m s^{-1}
u_{zm}	Wind speed at measuring height		m s^{-1}
p	Atmospheric pressure		Pa
p_d	Partial pressure		Pa
q	specific humidity		
z	Height/Depth		m
z_m	Measuring height		m
z_{mix}	depth of mixed layer		m
z_g	depth of centre of gravity		m
z_0	Roughness length	10^{-4} [h]	m
α_w	Surface reflectance (albedo) of water	0.05	
α_s	Surface reflectance (albedo) of snow	0.90[i]	
α_i	Surface reflectance (albedo) of ice	0.55[h]	
β_w	Surface absorption of water	0.4[j]	
β_i	Surface absorption of ice	0.4[i]	
β_s	Surface absorption of snow	0.4[i]	
θ_j	fraction of material		
$\theta_{w(min)}$	minimum water fraction		
$\theta_{w(max)}$	maximum water fraction		
ε_w	surface emissivity of water	0.97[j]	
ε_s	surface emissivity of snow	0.85[k]	
ε_i	surface emissivity of ice	0.96[k]	
κ	von Kármán constant	0.4	
ρ_{air}	Density of humid air		kg m^{-3}

[g] Riche, F., and M. Schneebeli (2013), Thermal conductivity of snow measured by three independent methods and anisotropy considerations, *The Cryosphere*, *7*, 217-227.

[h] Garratt, J. R. (1994), *The atmospheric boundary layer*, Cambridge university press.

[i] Gu, R., and H. G. Stefan (1990), Year-round temperature simulation of cold climate lakes, *Cold Regions Science and Technology*, *18*(2), 147-160.

[j] Riley, M. J., and H. G. Stefan (1987), *Dynamic lake water quality simulation model" MINLAKE"*, St. Anthony Falls Hydraulic Laboratory, University of Minnesota.

[k] http://www.infrared-thermography.com/material-1.htm

ρ_{ice}	Density of ice	916.7[l]	kg m^{-3}
ρ_w	Density of water		kg m^{-3}
ρ_s	Density of Snow	250[g]	kg m^{-3}
ω	Turbulence dependent parameter	6.9 e^{-6}	

[l] Lide, D. R. (2012), *CRC handbook of chemistry and physics*, CRC press.

A.2. Model Setup

Table A.2 Soil composition

Depth (m below WS)	0	*Bottom of water body*	15	500
$\theta_{w(max)}$	1	1	0.7	0.3
θ_m	0	0	0.2	0.7
θ_o	0	0	0.1	0
$\theta_{w(min)}$	0	0	0.04	0.04

A.3. Wind induced mixing

Shear velocity of water induced by wind is calculated as [*Riley and Stefan*, 1987]

$$u^* = 0.0343\sqrt{C_z}u_w, \tag{25}$$

with C_z an empirical coefficient depending on wind speed u_w

$$C_z = \begin{cases} 0.0005\sqrt{u_w} & for \quad u_w < 15\ ms^{-1} \\ 0.0026 & for \quad u_w \geq 15\ ms^{-1} \end{cases}, \tag{26}$$

The wind speed at the water surface is computed from the measured wind speed over land using the similarity of the logarithmic wind profile

$$u_w = u_l \frac{\ln\frac{z_m}{z_{02}} \ln\frac{z_b}{z_{01}}}{\ln\frac{z_m}{z_{01}} \ln\frac{z_b}{z_{02}}}, \tag{27}$$

with u_l the wind speed over land, z_m measuring height, z_{01} surface roughness of land (10^{-2}), z_{02} surface roughness over water (10^{-4}) and z_b the equivalent boundary layer over the water calculated as

$$z_b = 0.34 Fetch^{0.8}, \tag{28}$$

$$Fetch = {}^{2}/_{3}\sqrt{{}^{A}/_{\pi}}, \tag{29}$$

A.4. Energy Balance

The dependency of air density on humidity and air temperature is accounted for by the use of the following equations:

$$\rho_{air} = \frac{p}{R_f \cdot T_{air}} \tag{30}$$

Where, p the atmospheric pressure, T_{air} the air temperature and R_f the gas constant of humid air obtained with

$$R_f = \frac{R_l}{1 - RH \cdot p_d/p \cdot (1 - \frac{R_l}{R_d})} \tag{31}$$

With, R_l the gas constant of dry air, RH the relative humidity, R_d the gas constant of water vapour. The saturation water vapour pressure p_d over a water surface can be obtained by the use of the Magnus formula [*Alduchov and Eskridge*, 1996]

$$p_d = 610.94Pa \cdot exp\left(\frac{17.625 \cdot T[^\circ C]}{243.04^\circ C + T[^\circ C]}\right) \quad for\ T > 0 \tag{32}$$

$$p_d = 611.21Pa \cdot exp\left(\frac{22.587 \cdot T[^\circ C]}{273.86^\circ C + T[^\circ C]}\right) \quad for\ T \leq 0 \tag{33}$$

A.5. Gap filled data

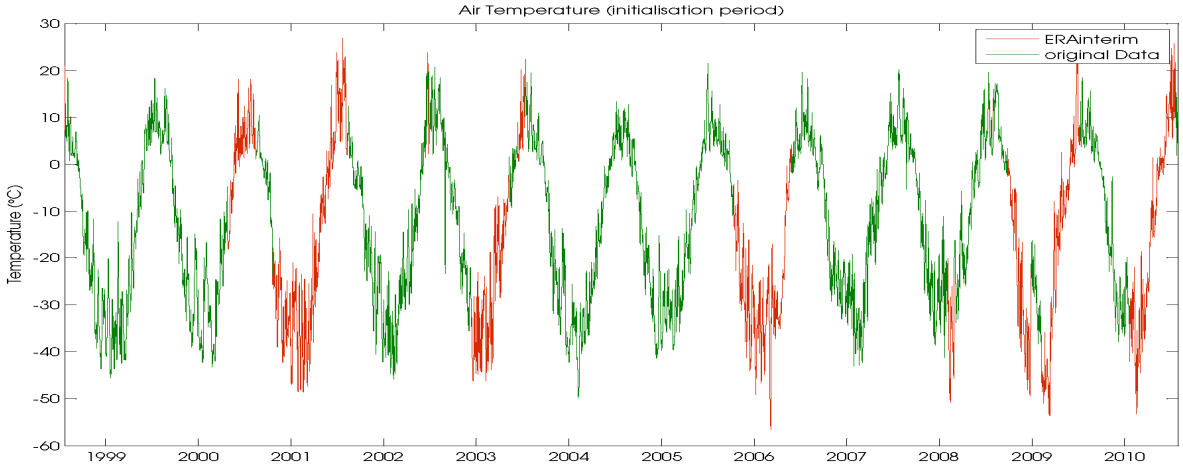

Figure A.1 Air temperature Aug 1998 to Aug 2010

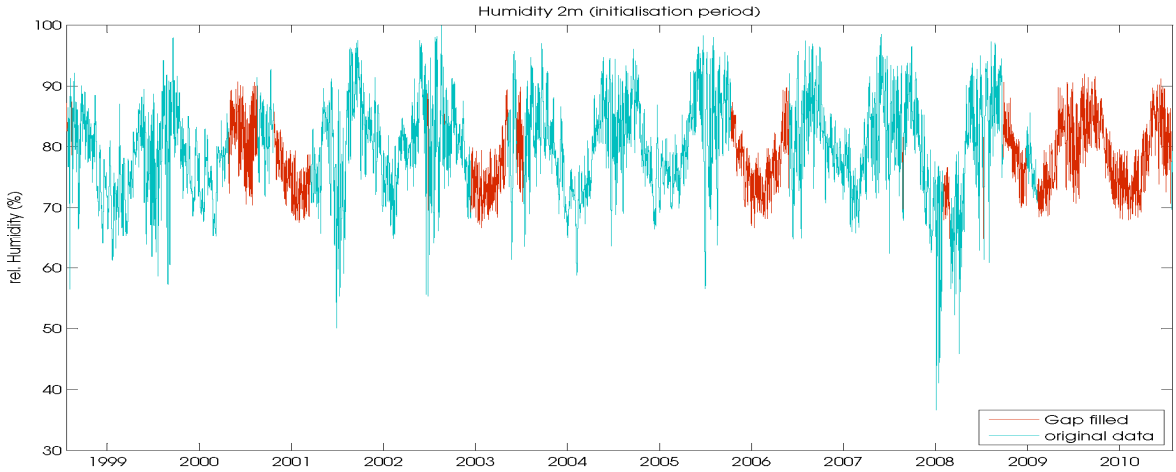

Figure A.2 Humidity Aug 1998 to Aug 2010

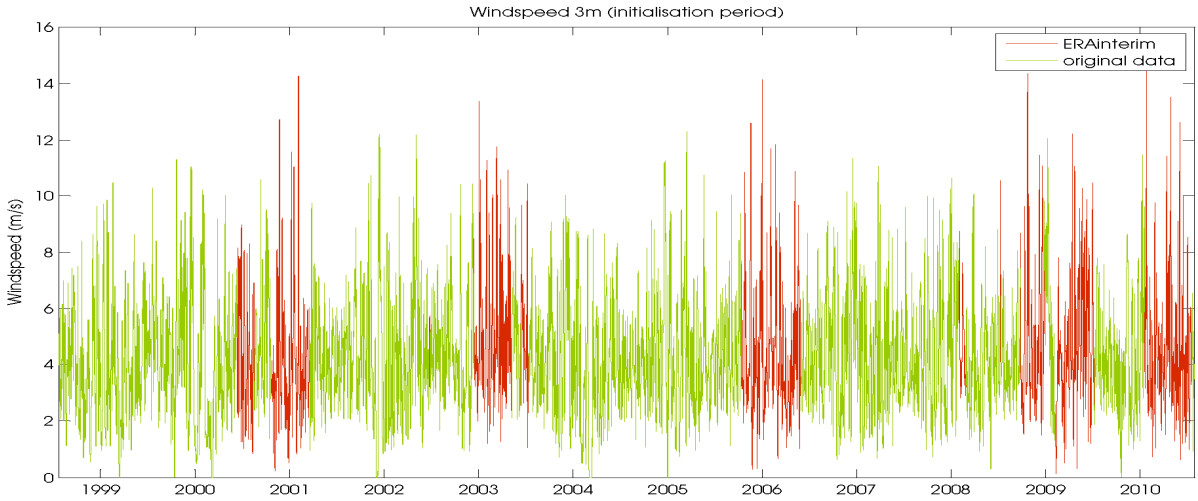

Figure A.3 Wind speed Aug 1998 to Aug 2010

A.6. Results

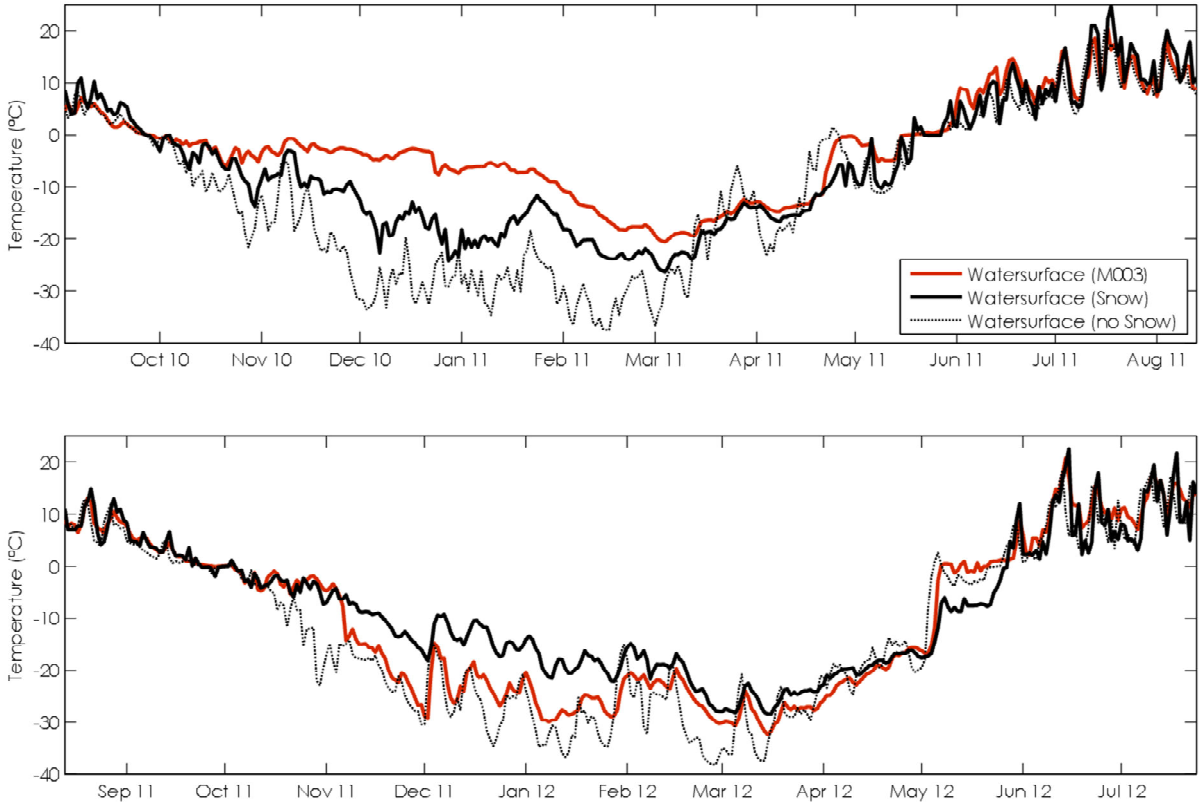

Figure A.4 Comparison of measured (red) temperatures water surface of M003 to simulated temperatures with snow cover (black) and without (dashed black).

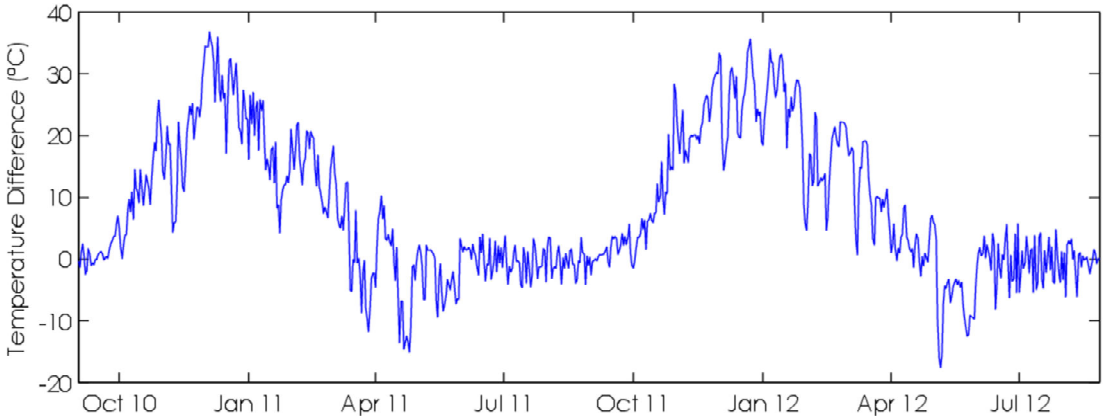

Figure A.5 Temperature difference between measured air temperature and temperature at the bottom of a pond with depth 0.81 cm

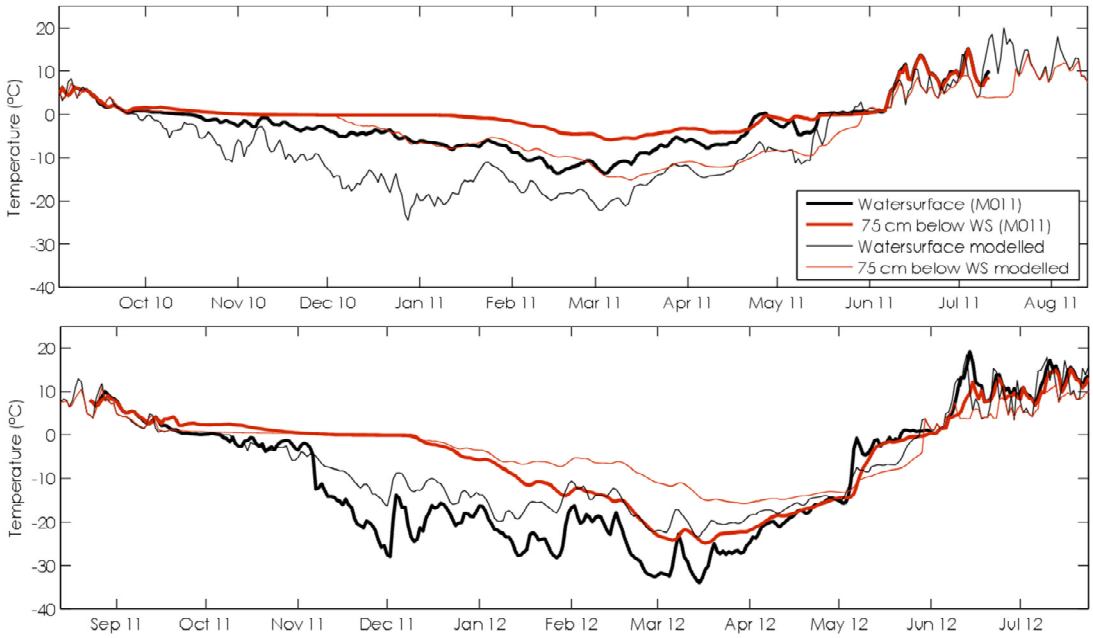

Figure A.6 Comparison of simulated (thin) and measured (thick) temperatures of a pond with depth 1.22 m, at the surface (black) and at 76 cm below water surface (red);.2010/11 (top) 2011/12 (bottom); upper boundary: air temperature & energy balance

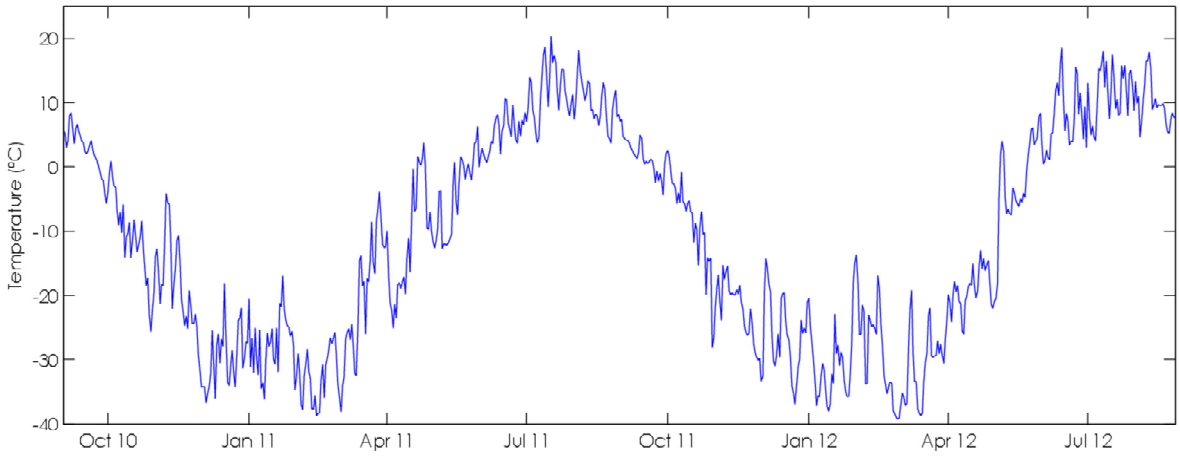

Figure A.7 Air temperature measured at climate station on Samoylov from 2010 to 2012

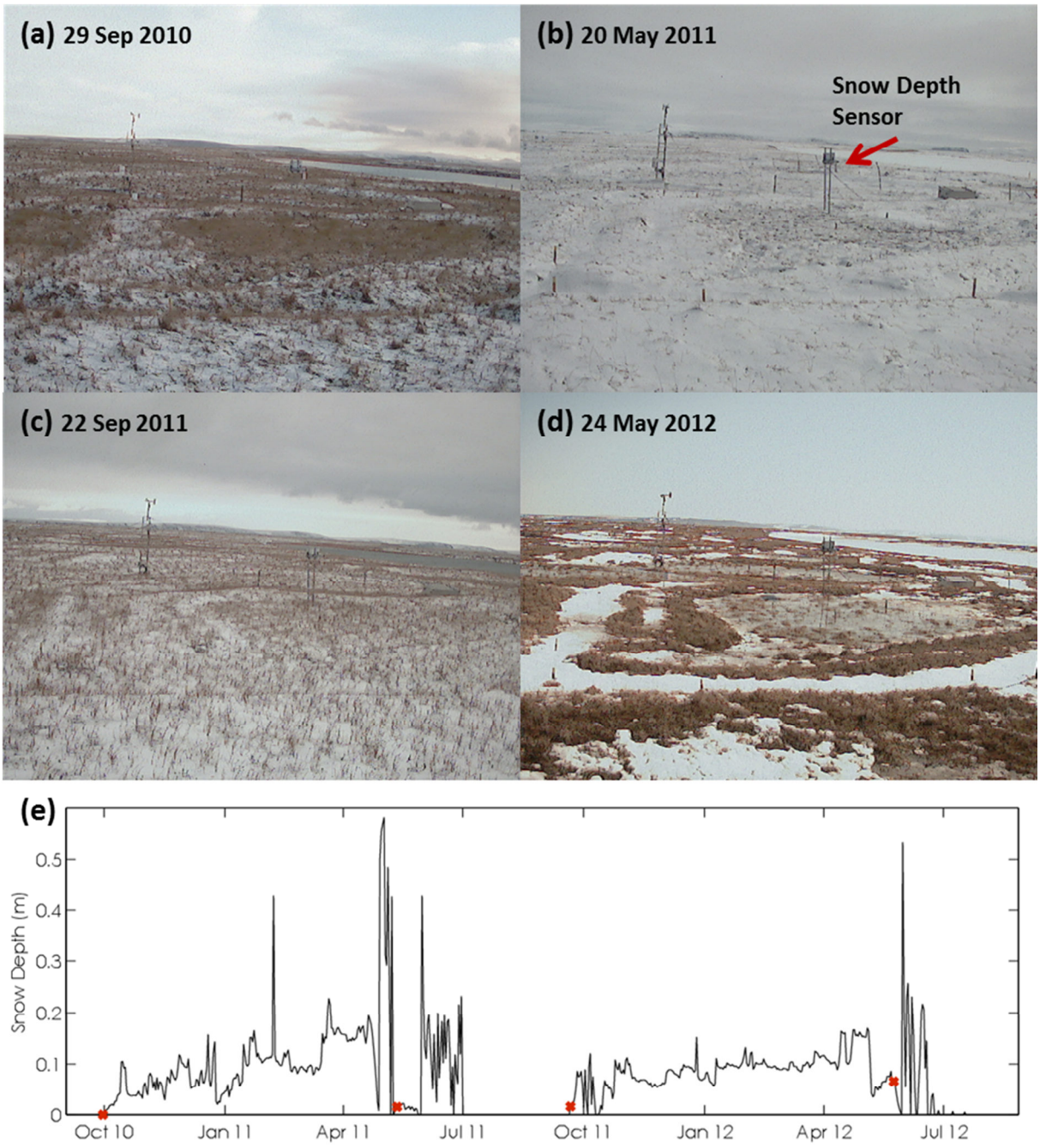

Figure A.8 Pictures from the automatic camera on Samoylov taken at 12 am (UTC +8) at a)+c) first day of snow cover and b)+d) last day of snow cover during 2010-2012; e) Snow depth measured at the centre of a polygon data with red markings for dates a)-d)

Acknowledgements

At this point I would like to thank a number of people without whom this would have been much harder.

Firstly I would like to thank my supervisor Julia Boike, who made this thesis possible and gave me valuable input and comments on my writings. Also I would like to thank the Alfred Wegener Institute Helmholtz Centre for Polar and Marine Research and many staff members to make my time on Samoylov Island possible and gave me the opportunity to collect field data.

Thank you, Prof. Wolfgang Kinzelbach for accepting this topic for my thesis and giving me very useful feedback in the discussions.

Special thanks are due to Moritz Langer who helped me through my modelling troubles and moments of desperation when everything seemed to go wrong. I thank you for your patience during our 'Skype-sessions' regardless of location or time.

Thank you Sina Muster, Max Heikenfeld, Niko Borneman and Roman Osudar to whom I could just go or call and talk about anything concerning my thesis or just life in general. It has been really refreshing. I would also like to thank Juliane Wischnewski and Miriam Brunke for the help with the English writing.

Last but not least I would like to thank my family and Manuel Helbig for helping and supporting me on so many other levels that it is hard to put it in words.